

# Oxidation Flow Reactor Results in a Chinese Megacity Emphasize the Important Contribution of S/IVOCs to Ambient SOA Formation

Weiwei Hu,\* Huaishan Zhou, Wei Chen, Yuqing Ye, Tianle Pan, Yingkun Wang, Wei Song, Huina Zhang, Wei Deng, Ming Zhu, Chaomin Wang, Caihong Wu, Chenshuo Ye, Zelong Wang, Bin Yuan, Shan Huang, Min Shao, Zhe Peng, Douglas. A. Day, Pedro Campuzano-Jost, Andrew T. Lambe, Douglas R Worsnop, Jose L. Jimenez, and Ximming Wang\*



Cite This: *Environ. Sci. Technol.* 2022, 56, 6880–6893



Read Online

ACCESS |

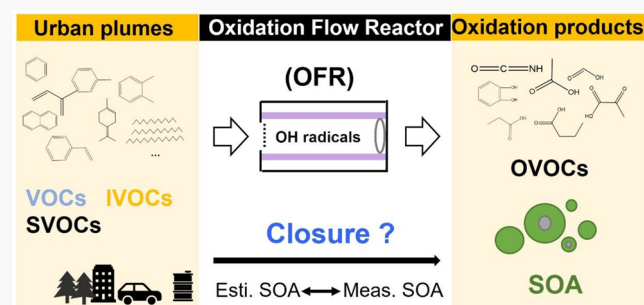
Metrics & More

Article Recommendations

Supporting Information

**ABSTRACT:** Oxygenated volatile organic compounds (OVOCs) and secondary organic aerosol (SOA) formation potential of ambient air in Guangzhou, China was investigated using a field-deployed oxidation flow reactor (OFR). The OFR was used to mimic hours to weeks of atmospheric exposure to hydroxyl (OH) radicals within the 2–3 min residence time. A comprehensive investigation on the variation of VOCs and OVOCs as a function of OH exposure is shown. Substantial formation of organic acids and nitrogen-containing OVOC species were observed. Maximum SOA formation in the OFR was observed following 1–4 equiv days' OH exposure. SOA produced from known/measured VOC/IVOC precursors such as single-ring aromatics and long-chain alkanes can account for 52–75% of measured SOA under low NO<sub>x</sub> and 26–60% under high NO<sub>x</sub> conditions based on laboratory SOA yield parametrizations. To our knowledge, this is the first time that the contribution (8–20%) of long-chain (C<sub>8</sub>–C<sub>20</sub>) alkane oxidation to OFR SOA formation was quantified from direct measurement. By additionally estimating contribution from unmeasured semivolatile and intermediate volatility compounds (S/IVOCs) that are committed with C<sub>8</sub>–C<sub>20</sub> alkanes, 64–100% of the SOA formation observed in the OFR can be explained, signifying the important contribution of S/IVOCs such as large cyclic alkanes to ambient SOA.

**KEYWORDS:** oxidation flow reactor, secondary organic aerosols, S/IVOCs, closure estimation, urban area, OVOC formation



## 1. INTRODUCTION

Organic aerosols (OA), accounting for 20–70% of the fine particle mass concentrations,<sup>1–3</sup> can substantially impact air quality, human health, and climate.<sup>4–7</sup> Despite its ubiquity, OA is still the least understood component of ambient aerosols due to its complex physicochemical properties that change as a function of atmospheric processing.<sup>8–10</sup> OA, comprised of thousands of individual species, can be directly emitted to the ambient air as primary organic aerosols (POA) or formed as secondary organic aerosols (SOA) through condensation from oxidation products of gas-phase organic precursors including volatile organic compound (VOC) and/or semi/intermediate VOC species (S/IVOC),<sup>8,11,12</sup> as well as from heterogeneous and multiple phase reactions.<sup>13,14</sup> Large discrepancies have been found between measured and simulated OA with various types of models in urban areas.<sup>15,16</sup> This large gap is mainly caused by the incomplete understanding of precursors, formation, and aging processes of SOA in urban plumes.<sup>17</sup>

Recently, the development of field-deployable oxidation flow reactors (OFR) has provided a new approach to investigate

SOA formation.<sup>18–21</sup> The advantages associated with OFR include its portability for investigating SOA formation in the field under real-world conditions, and access to a wide range of OH exposures (several hours to months) within minutes of real time.<sup>22–27</sup> The latter enables the study of the multi-generational SOA oxidative aging process including formation of early generation, lower volatility oxidation products followed by later-generation, and higher-volatility oxidation products formed from fragmentation reactions which also can result in net SOA mass losses.<sup>14,28,29</sup>

So far, OFR field studies include measurement locations at forest areas,<sup>23,24,29,30</sup> urban downtown,<sup>22,26,27,31,32,33</sup> roadside,<sup>26,32</sup> tunnel environments,<sup>25</sup> and aircraft.<sup>34</sup> Those studies

**Special Issue:** Urban Air Pollution and Human Health

**Received:** May 19, 2021

**Revised:** November 15, 2021

**Accepted:** November 17, 2021

**Published:** December 13, 2021



found up to a factor of 4 increase in the SOA:POA ratio as a function of OH exposure in OFR. Further, OH oxidation of traditional VOC precursors in OFRs is thought to contribute only a fraction (~20–50%) of the observed SOA formation, with remaining SOA formation typically attributed to the oxidation of S/IVOCs and oxygenated VOCs (OVOCs) with potentially large SOA yields as in ambient SOA formation.<sup>22,25,27,35,36</sup>

Overall, contributions of S/IVOCs to SOA formation in real-world urban environments are poorly constrained due to the analytical challenges associated with measurements, their variable emission factors from different sources, and overall low level of characterization in laboratory chamber studies relative to VOCs.<sup>37,38</sup> For example, Lu et al.<sup>39</sup> showed S/IVOCs emitted from sources such as diesel, gas-turbine engines have substantially higher SOA formation potential than traditionally well-studied VOCs such as monoaromatics, whereas S/IVOC and traditional VOC emissions from gasoline engine contribute similar amount to SOA formation. Similarly, while some box<sup>22,40</sup> and 3-D<sup>41</sup> modeling work show important S/IVOC contributions to SOA formation in urban environments, other models<sup>42–44</sup> found less. In situ OFR-based studies of the SOA formation potential in urban regions, coupled with direct measurements of both reactive VOC and S/IVOC precursors, may provide new insight on this issue.

In this study, we investigated the in situ OVOC and SOA formation potential of ambient air at a typical urban area in China using an OFR. A comprehensive suite of VOCs and primary and secondary OVOCs were measured as a function of OH exposure. Similarly, secondary organic and inorganic aerosol formation was characterized as a function of photochemical age and compared with results from previous OFR studies. The combined set of gas- and condensed-phase measurements was used to estimate contributions of individual SOA precursor to the observed SOA formation in the OFR. Notably, for the first time, we estimated SOA contributed from C<sub>8</sub>–C<sub>20</sub> alkanes, where C<sub>12</sub>–C<sub>20</sub> alkanes are key IVOC species, based on direct measurement of their consumption in the OFR.

## 2. EXPERIMENTAL SECTION

**2.1. Field and Laboratory Experiments.** The field campaign PRIDE-GBA (Particles, Radicals, Intermediates from oxiDation of primary Emissions in Greater Bay Area) was conducted in Guangzhou city, China from October to November 2018.<sup>45</sup> The observation site (23.13°N, 113.26°E), located in a typical downtown urban area, was on the roof of a 9-story building in the campus of Geoscience Institute at Guangzhou (GIG), Chinese Academy of Science (CAS) (**Supporting Information (SI) Figure S1**). Ambient temperature and relative humidity (RH) during the campaign ranged from 17 to 31 °C (23.7 ± 2.8 °C in average) and 40 to 95% (72 ± 17%), respectively.

**2.2. Oxidation Flow Reactor (OFR).** **SI Figure S2** shows a schematic of the OFR-based experimental setup. During PRIDE-GBA, ambient air was exposed to OH radicals generated in an aerodyne potential aerosol mass (PAM) OFR.<sup>18–20</sup> The PAM OFR is a cylindrical vessel with an internal volume of 13.3 L. Two low pressure mercury UVC lamps covered by segmented heat shrink tubing were enclosed in type 214 quartz sleeves and mounted symmetrically in the opposite corners of the OFR (**SI Figure S2**). A nitrogen purge gas flow of 0.2–0.3 L min<sup>-1</sup> was introduced into the sleeves to

cool the lamps and to prevent ozone formation between the lamps and sleeves.<sup>23,29</sup>

OH and HO<sub>2</sub> radicals were generated via photolysis of O<sub>2</sub> + H<sub>2</sub>O at  $\lambda = 185$  nm plus photolysis of O<sub>3</sub> at  $\lambda = 254$  nm.<sup>46–48</sup> The RH and temperature in ambient air and the OFR were monitored by an ambient meteorological station on site and a sensor set in the backplate of OFR (**SI Figure S3**). A fluorescent dimming ballast was used to control the photon flux and OH concentration by regulating the voltage applied to the lamps through the control software. In typical measurement sequences, we cycled through eleven lamp voltage settings (including light off) every 2–3 h.

To maximize transmission of ambient gas and aerosol species through the OFR inlet, a 1.5 m-long conductive PFA tube (1/4 in., o.d.) wrapped with aluminum foil was used based on the results of Deming et al.<sup>49</sup> Gases and particles were sampled from the OFR through separate Teflon and stainless-steel sample lines, as shown in **SI Figure S2**. A makeup flow was added to maintain constant flow through the OFR and ambient sampling line to minimize dead volumes. The OFR was sampling ambient air all the time. The total flow rates through the OFR were between 4.7 and 7.5 L min<sup>-1</sup> depending on instrument deployment after OFR at different periods during field measurements corresponding to a calculated mean residence time of 110–170 s. Within the residence time range, no kinetic limitation for condensation of SVOC/LVOC was found due to the high ambient condensation sink in this study (OA concentration is >1.5  $\mu\text{g m}^{-3}$ ).<sup>50,51</sup>

**2.3. Instrumentation.** The chemical composition of ambient and oxidized aerosols in OFR were detected by a high-resolution time-of-flight aerosol mass spectrometer (HR-ToF-AMS, hereafter termed as “AMS”, Aerodyne Research Inc. Billerica, MA) coupled with standard vaporizer (SV)<sup>52</sup> at a time resolution of 2 min.<sup>53,54</sup>

The ionization efficiency (IE) of the AMS was calibrated every 3–5 days with monodisperse 400 nm dry pure ammonium nitrate particles (NH<sub>4</sub>NO<sub>3</sub>). A stable IE/airbeam variation across the entire campaign (<5%) was found. Two Nafion dryers (Puma Pure Inc., U.S.) were used to maintain sample RH < 40% before entering the AMS. A chemical composition-based collection efficiency (CDCE) correction was applied to the AMS data sets.<sup>55</sup> OA elemental ratios were obtained by fitting the high-resolution peaks of ions detected by ToF-MS, and corrected with the new calibration parameters reported in Canagaratna et al.<sup>56</sup>

In addition to the AMS, a scanning mobility particle sizer (SMPS) was used to measure particle size distribution (mobility diameter = 14–650 nm) at a time resolution of 4 min. The total residence time of the ambient sampling line to the AMS and SMPS was ~3 s, and a 30 s delay ahead of data acquisition was applied when alternating between OFR and ambient lines to avoid air-lag influences from nucleation explosion from OFR. **SI Figures S4 and S5** show good agreement on particle mass concentrations between the AMS vs SMPS measurements.

A proton-transfer reaction time-of-flight mass spectrometer alternating between H<sub>3</sub>O<sup>+</sup> and NO<sup>+</sup> ion chemistry (referred to “PTR-MS” hereafter, Ionicon Analytik and Kore Technology, Austria)<sup>57,58</sup> and an iodide-adduct long time-of-flight chemical-ionization mass spectrometer (referred to “I-CIMS”, Aerodyne Research Inc., U.S.)<sup>59</sup> were used to measure VOCs, IVOCs, and OVOCs from November 9 to November 20 with 10–30 s time resolution. The PTR-MS was calibrated daily with a 16-

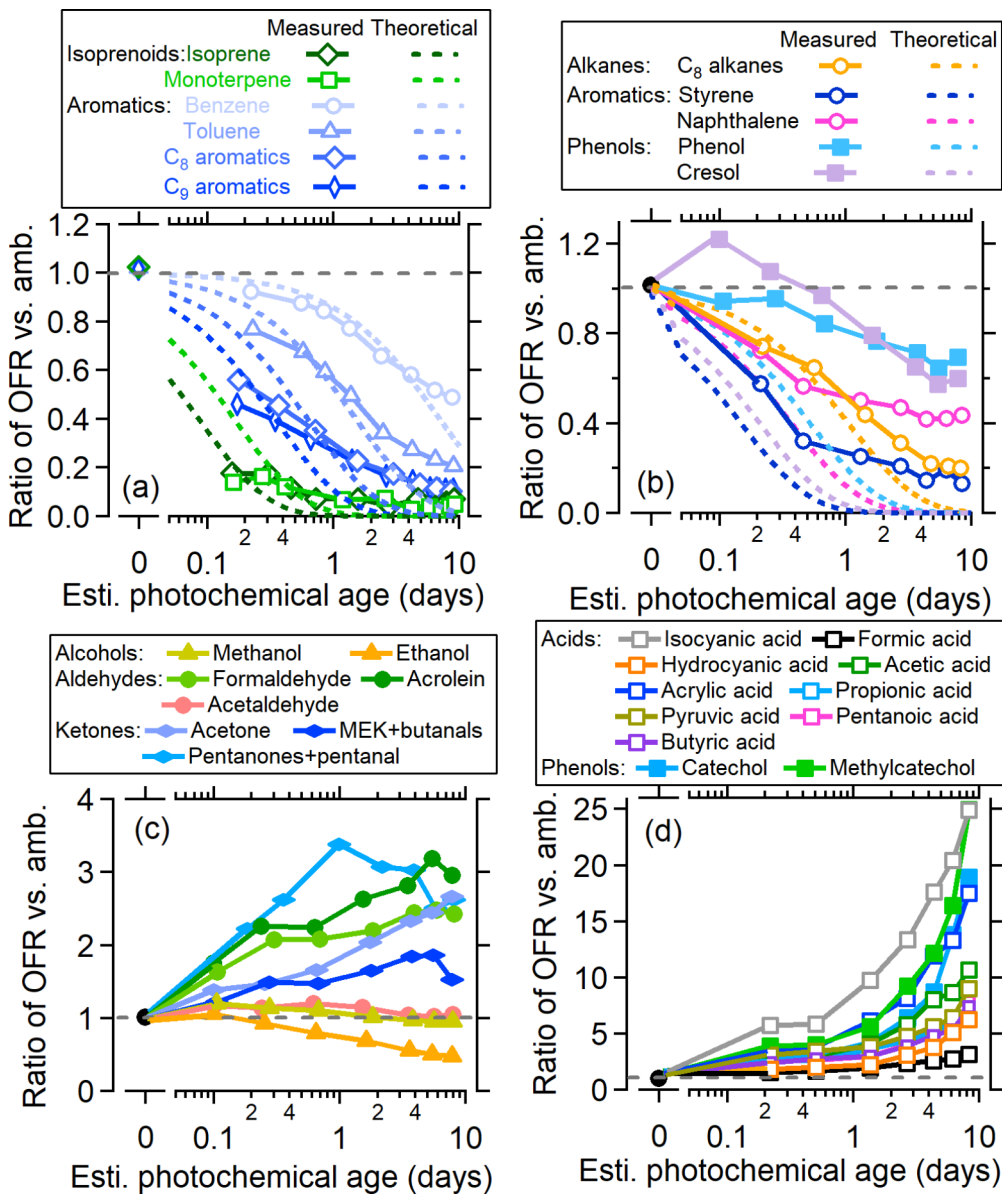


**Figure 1.** Relative ratios of gas-phase organic compound concentration between OFR and ambient air as a function of atmospheric-equivalent photochemical age in OFR. In Figure 1a,b, theoretical decays were also calculated with the  $k_{\text{OH}}$  from literatures assuming VOCs only react with OH radicals, and assuming laminar flow with the measured RTD shown in SI Figure S8. All the VOC species were measured by the PTR-MS and CIMS. Detailed information on instrumentation,  $k_{\text{OH}}$  used for different VOC species can be found in SI Tables S1 and S2.

component VOC gas standard mix under both dry and ambient RH.<sup>45</sup> In calibrating mixing ratios of OVOCs measured with the CIMS, a voltage scanning procedure was performed after consideration of relative transmission efficiency for the ions. Detailed information on this CIMS calibration can be found in a separate instrument overview paper in Ye et al.<sup>59</sup> This assumption does not change interpretation of trends in individual compounds as a function of OH exposure but may bias the calculated relative abundances of individual OVOCs. Mean mixing ratios, proposed molecular structures, and OH reaction rate coefficients ( $k_{\text{OH}}$ ) are summarized in SI Tables S1 and S2. O<sub>3</sub> were measured with an O<sub>3</sub> analyzer (model 205 dual beam, 2B Technologies Inc., U.S.) at a time resolution of 10 s.

**2.4. Wall Loss and LVOC Fate Correction.** Losses of gas and aerosol species to OFR walls were calculated by normalizing their mass concentrations measured in OFR

with the lights turned off to corresponding mass concentrations measured through the ambient sample line immediately before and after sampling the dark OFR.<sup>23</sup> Negligible wall losses were observed for VOCs, IVOCs, and small organic acids measured with the PTR-MS and CIMS (SI Table S2). The wall loss correction for low volatile organic compounds (LVOCs), which are oxidized products from VOCs, was also performed according to the estimation method in Palm et al.<sup>23</sup> In this study, an upper limit of only 20% of the LVOCs was lost to the wall due to the high condensation sink of aerosols in OFR (SI Figure S6). For consistency with previous studies,<sup>22,23</sup> all LVOC fate correction including LVOC wall loss, gas-reaction of LVOCs with OH radicals, and LVOC exiting OFR pathways were corrected to the final SOA mass concentration in OFR. In the model, we assumed the formed SOA was predominately contributed by the LVOC, similar to Palm et al.<sup>23</sup>

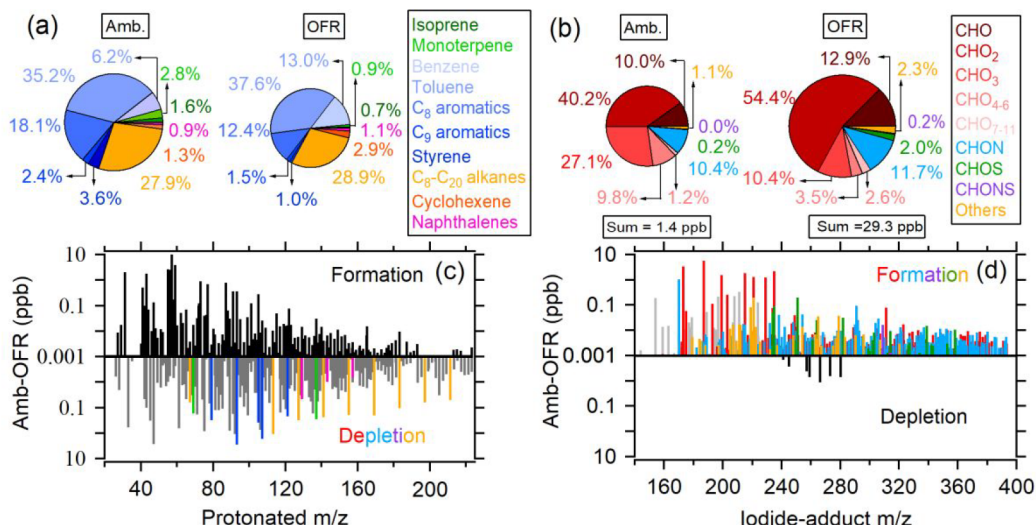


**Figure 2.** VOC composition in ambient and OFR measured by (a) the PTR-MS and (b) the CIMS at a typical time point (November 18, 17:00–18:00). The isoprene and C<sub>8</sub>–C<sub>20</sub> alkanes in Figure 2a,c were measured by PTR-MS NO<sup>+</sup> mode, and others are from PTR-MS H<sub>3</sub>O<sup>+</sup> mode. The OH<sub>exp</sub> in the OFR is equivalent to ~4 days of photochemical ages. This data point shows a comparison ratio of ~1:1 between RO<sub>2</sub>+HO<sub>2</sub> versus RO<sub>2</sub>+NO ratio. We classified the measured VOC species into different categories by their assigned molecular structure in PTR-MS. The category of the CIMS was based on ion elemental composition. Mass spectrum differential of gas-phase organic species between ambient and OFR in the (c) PTR-MS and (d) CIMS. The color code is consistent with their corresponding pie charts. The black and gray sticks in Figure 2c are the formed ions and depleted ions in the PTR-MS without categorization as shown in Figure 2a. The black ions in Figure 2d is the depleted ions detected by the CIMS.

We measured campaign-average wall losses of 5% for OA, and 1% for sulfate, 28% for nitrate, and 41% for chloride aerosols detected with the AMS (SI Figure S7). Our OA wall losses are similar to values (4–5%) reported in other ambient PAM OFR studies.<sup>22,23,29,34</sup> The strong positive correlation between nitrate and chloride loss with RH suggested the high RH is the leading factor for OFR denuding effect in this study (SI Figure S8). This might be due to the nitrate and chloride are more sticky to the wet internal wall at higher RH.

**2.5. Estimated Contribution of VOC and IVOC Precursors to SOA Formation in OFR.** To estimate the SOA contributed from VOC and IVOC consumption in the OFR that was measured with PTR-MS, we applied laboratory SOA yield parametrizations based on 4-product<sup>38,44</sup> and 5-product<sup>60</sup> volatility basis set (VBS) distributions of the effective saturation concentration (C\*) at 298 K (SI Table S3). Because SOA yields are in some cases influenced by NO<sub>x</sub> levels, laboratory SOA mass yields obtained in both low and high NO<sub>x</sub> chemistry regimes were applied in this analysis as upper and lower limit values. The laboratory SOA mass yield under high NO<sub>x</sub> condition already include the SOA masses from organic nitrate contribution. We used a box model<sup>51</sup> to simulate the RO<sub>2</sub> fate in OFR under our field study condition. The results showed when only HO<sub>2</sub> and NO pathways were compared, an average  $21\% \pm 17\%$  of RO<sub>2</sub> reacted with NO and left with HO<sub>2</sub> (79%) in the OFR of this campaign (SI Figure S9a) by assuming a reaction rate coefficient of 1e-11 cm<sup>3</sup> molecule<sup>-1</sup> s<sup>-1</sup> for both reactions. The dominance of HO<sub>2</sub> oxidation pathway with RO<sub>2</sub> is mainly due to the NO<sub>x</sub> quick oxidation by OH, HO<sub>2</sub>, and O<sub>3</sub> reactions in the OFR under high OH exposures (>5 days) suppress the role of NO<sub>x</sub> in OVOC and SOA formation in our studies.<sup>51,61</sup> However, the fraction of NO pathway could increase up to 80–95% as the ambient NO concentration got higher and OH equivalent aging time is below 2 days, as shown in SI Figure S9b.

**2.6. OFR OH Exposure Calibration in the Laboratory and Field Studies.** The integrated OH exposure (OH<sub>exp</sub>), defined as the product of the mean OH concentration and OFR residence time, was calculated from the decay of reactive gas-phase tracers<sup>46,48</sup> using a setup as shown SI Figure S2b and laboratory experimental conditions summarized in SI Table S4. Based on these series of OH<sub>exp</sub> calibration experiments, a set of parameters (SI Table S5) for empirical OH<sub>exp</sub> estimation eq (SI eq S1) was recalibrated. The detailed calibration procedure and results can be found in SI Section 1. Overall, both laboratory with standard gases of SO<sub>2</sub> and VOCs (SI Figures S11–S15) and field studies (Figure 1a) show the new set of parameters obtained here is applicable for estimating the OH<sub>exp</sub> in field-deployed OFR when RH is >20%.

### 3. RESULTS AND DISCUSSIONS

**3.1. VOC Oxidation and OVOC Formation in OFR.** Figure 1 shows the study-average behavior of representative VOCs, IVOCs, and OVOCs measured as a function of OH exposure in the OFR. Concentrations of primary VOCs such as alkanes, aromatics and isoprenoids decrease in the OFR relative to their ambient levels (Figure 1a,b). The rate of decay of these primary VOCs generally tracks the theoretical decay curves calculated from their literature k<sub>OH</sub> values (SI Table S1) and the OH exposure in the OFR. For example, benzene ( $k_{OH} = 1.22 \times 10^{-12}$  cm<sup>3</sup> molec.<sup>-1</sup> s<sup>-1</sup>) decays the slowest whereas isoprene and monoterpene ( $k_{OH} = 1.0 \times 10^{-10} - 5.23 \times 10^{-11}$  cm<sup>-3</sup> molec.<sup>-1</sup> s<sup>-1</sup>) decay much faster.

The wide spectrum changes of overall organic species in ambient vs OFR during a typical period is shown in Figure 2. The largest absolute VOC decay was associated with toluene (Figure 2a), due to its high ambient concentrations<sup>57,58</sup> and moderate k<sub>OH</sub> value<sup>62</sup> (SI Table S1) that enabled significant consumption in the OFR over the range of OH<sub>exp</sub> studied here. For similar reasons, significant consumption of other aromatic

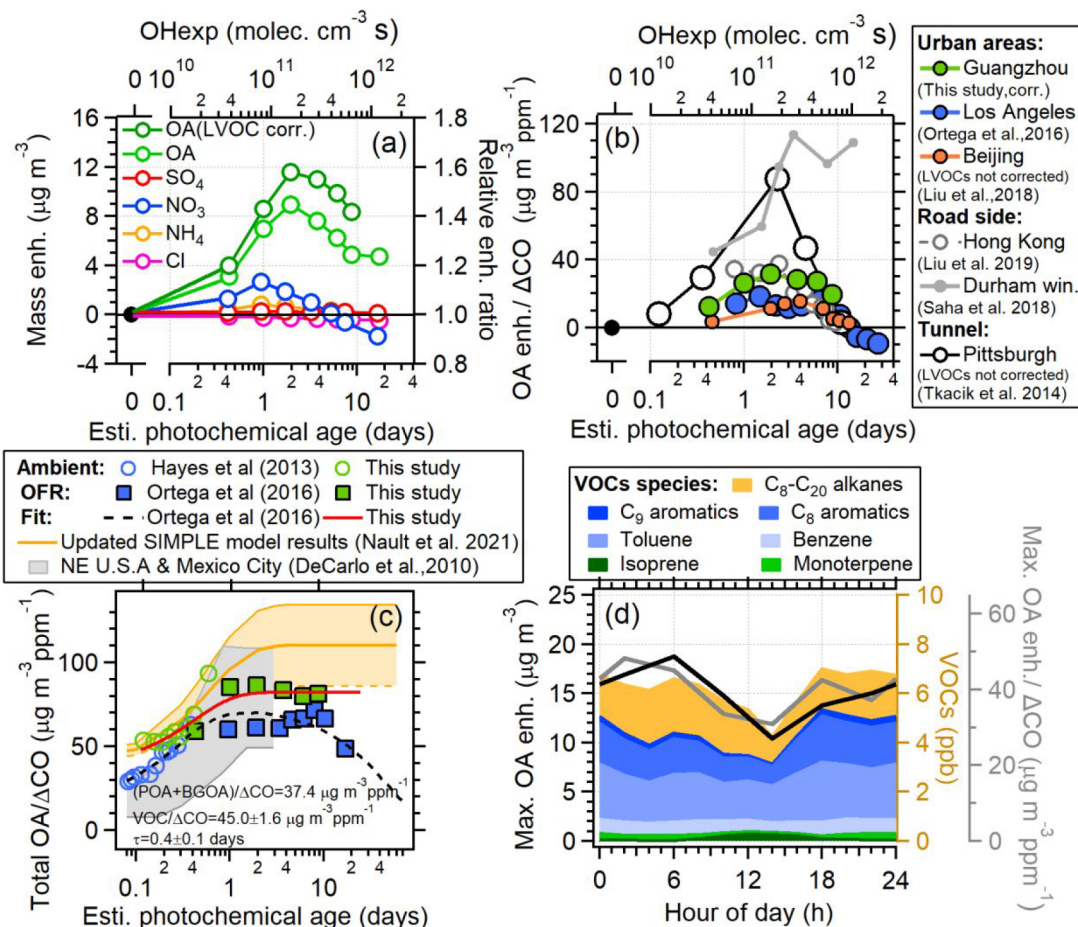


**Figure 3.** (a) Enhancement of absolute mass concentration of OA and other inorganic species (sulfate, nitrate, ammonium, and chloride) as a function of estimated photochemical age, assuming ambient OH concentration =  $1.5 \times 10^6$  molec.  $\text{cm}^{-3}$ .<sup>79</sup> Corrected enhanced OA enhancement results using a LVOC fate model<sup>23</sup> are also shown. The enhanced OA data used in subsequent analysis of this study are all LVOC fate corrected. The scaled enhancement ratio is shown on the right axis. (b) Enhanced OA /  $\Delta\text{CO}$  (i.e.,  $\Delta\text{OA}/\Delta\text{CO}$ ) as a function of photochemical age at Guangzhou and comparison with OFR results obtained in other anthropogenic influenced areas. Note LVOC wall loss from the Beijing study<sup>31</sup> and Tunnel study in Pittsburgh<sup>25</sup> were not corrected, although the correction should be small (<20%) based on their high aerosol concentrations.<sup>23</sup>  $\Delta\text{CO}$  = measured CO – background CO (135 ppb) was used in this study (c) Comparison of total OA /  $\Delta\text{CO}$  versus photochemical age at Guangzhou and Los Angeles studies.<sup>22</sup> The total OA in OFR is the sum of ambient OA and newly formed OA. Equation 1 was used to fit the line. Fitted parameters are shown in Figure 3c. The SIMPLE model was calculated based on updated correlation between VOC emission ratio and normalized Monoaromatic VOC reactivity (sum of benzene, toluene and C8 reactivity versus  $\Delta\text{CO}$ ) reported in Nault et al.<sup>47</sup> The detailed introduction about SIMPLE model can be found in Hodzic and Jimenez et al.<sup>41</sup> (d) The diurnal variation of maximum OA enhancement and  $\Delta\text{OA}/\Delta\text{CO}$  in the OFR, and the diurnal variations of ambient VOC and IVOC concentration measured by PTR-MS are also shown. The diurnal variation time in the x-axis of Figure 3d refers to local time.

species such as C<sub>8</sub>, C<sub>9</sub> aromatics, benzene, and styrene was observed (Figure 2).

On the other hand, compounds such as phenol and cresol decayed more slowly than expected based on their  $k_{\text{OH}}$  values (Figure 1b). The formation of cresol was found in OFR at low OH exposures (<1 equiv day). This behavior is observed because these compounds are emitted directly from primary sources yet are also important first- and second-generation oxidation products that are formed from the reaction of benzene and toluene with OH and HO<sub>2</sub> radicals.<sup>63–65</sup> At higher OH exposure, oxidation of phenol and cresol resulted in large production of later generational oxidation products such as catechol and methyl catechol whose concentrations were enhanced by up to 20–25 at an equivalent photochemical age of ~10 days (Figure 1d).

Additionally, C<sub>1</sub>–C<sub>5</sub> OVOCs were detected at enhanced levels in the OFR, including carbonyls such as formaldehyde (CH<sub>2</sub>O), acetone (C<sub>3</sub>H<sub>6</sub>O), acrolein (C<sub>3</sub>H<sub>4</sub>O), and acids such

as formic acid (CH<sub>2</sub>O), acetic acid (C<sub>2</sub>H<sub>4</sub>O), butyric acid (C<sub>4</sub>H<sub>8</sub>O<sub>2</sub>), pyruvic acid (C<sub>3</sub>H<sub>4</sub>O<sub>3</sub>), pentanoic acid (C<sub>5</sub>H<sub>10</sub>O<sub>2</sub>), isocyanic acid (HNCO) and hydrocyanic acid (HCN) (Figure 1c,d and Figure 2). These compounds are known oxidation products of biogenic<sup>23,66</sup> and anthropogenic VOCs.<sup>67–69</sup> Here we hypothesize that these organic acids formation are formed primarily from multigenerational oxidation of VOCs<sup>70,71</sup> and/or heterogeneous oxidation of particles,<sup>72</sup> with potentially very minor contributions from OA photolysis (<1% of total OA) at 185/254 nm.<sup>47,73</sup>

Among all the molecules measured by the CIMS (Figure 2 and SI Figure S15) OVOCs with 1–2 oxygen atom (C<sub>x</sub>H<sub>y</sub>O and C<sub>x</sub>H<sub>y</sub>O<sub>2</sub>) are the mostly increased molecules (a factor of 30 for absolute concentrations), the fraction of which increased from 55% to 80% as the absolute total OVOC concentration enhanced 20 times in OFR. Less formation of OVOCs containing 3–6 oxygen atoms (a factor of 7.5) was observed. Large amount of newly formed OVOCs with seven or more

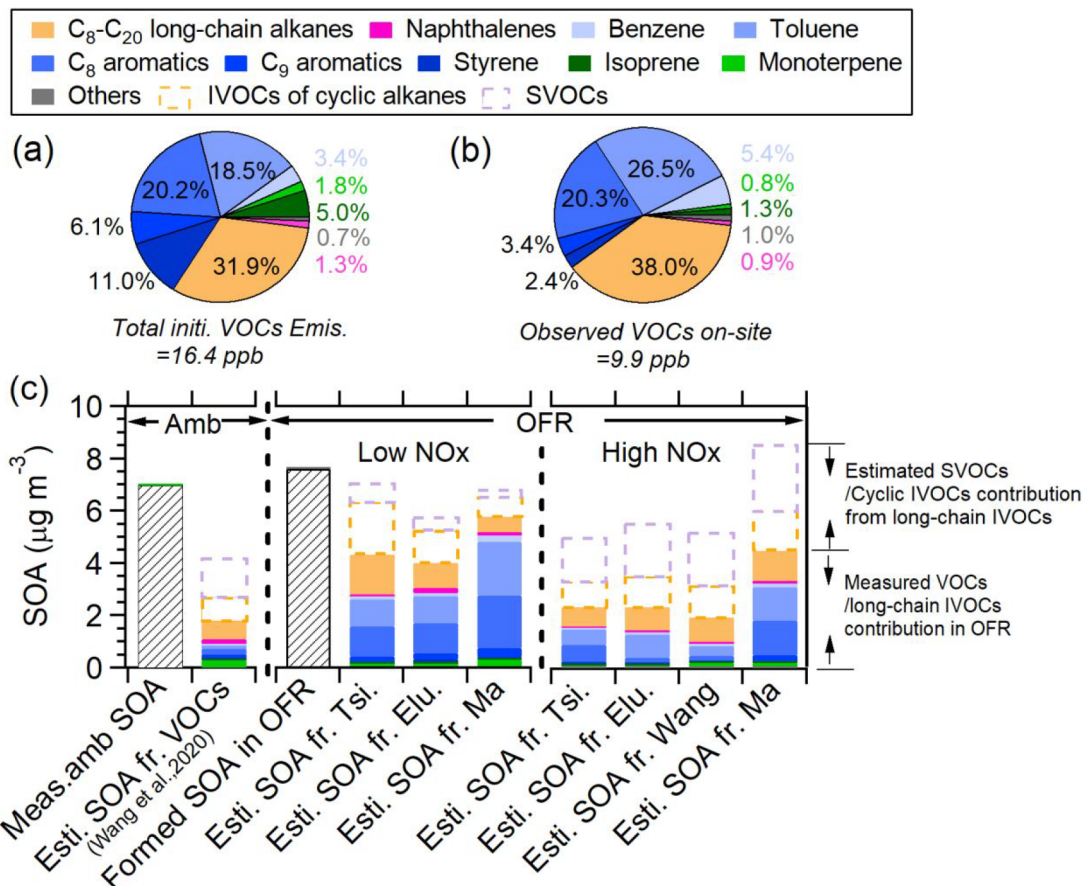


**Figure 4.** (a) Composition of initial VOC emissions in ambient air, which was obtained by averaging VOC results when photochemical age = 0 (b) Measured ambient VOC composition, which is also the OFR input. All the VOC data were obtained based on PTR-MS measurement (see details in SI). (c) Measured SOA versus predicted SOA in ambient and OFR. SOA mass yield from high and low  $\text{NO}_x$  chemical regions are both shown here. Tsi,<sup>44</sup> Elu,<sup>60</sup> Wang,<sup>57</sup> Ma<sup>38</sup> refer to different parametrizations of SOA yields from literature (SI Table S3). LVOC fate correction has been applied to the measured SOA concentration in OFR. The solid color bars represent the SOA estimated based on the observed consumption of VOCs and  $\text{C}_8\text{--C}_{20}$  linear alkanes in OFR. The orange and purple dashed line bars represent the SOA contributed from cyclic alkanes and SVOCs constrained based on SOA formation from  $\text{C}_8\text{--C}_{20}$  linear alkanes.

oxygen atoms (7.6 ppb, a factor of 40 enhancement) were also found. The highly oxidized molecules may be generated following autoxidation of peroxy radicals, especially under low OH exposure,<sup>51</sup> and have been observed following the OH oxidation of aromatic and olefinic VOCs.<sup>68,74</sup>

Finally, the fraction of nitrogen and sulfur-containing OVOCs also increased from 0.15 to 3.4 ppb (a factor of 22) and from 0.002 to 0.58 ppb (a factor of >100), respectively, with OH exposures. (Figure 2). Isocyanic acid (HNCO), a toxic compound for human health,<sup>75</sup> is the most enhanced nitrogen-containing species. The greatly enhanced ratio of HNCO in OFR (up to a factor of 25) supports that photochemistry is an important formation pathway for ambient HNCO under urban environments.<sup>76,77</sup>

**3.2. Secondary Aerosol Formation in OFR.** Time series and the average mass concentration of OA in the ambient air and OFR are shown in SI Figure S18. Much higher SOA formation was observed in the OFR during polluted periods (a factor of 2.6), with elevated concentrations of ambient aerosols and VOC precursors, than clean periods (SI Figure S18e). The high SOA formation potential measured in the OFR during polluted periods suggests that the full impact of haze events is realized over extended atmospheric aging time scales that are relevant to regional transport.

Figure 3 shows the average absolute enhancement in aerosol mass concentrations (OFR output, ambient) as a function of  $\text{OH}_{\text{exp}}$ . The OA enhancement increased rapidly at lower  $\text{OH}_{\text{exp}}$  and peaked around 2 equiv days (peak conc. =  $11.5 \mu\text{g m}^{-3}$ ) due to efficient condensation of semivolatile and low-volatility oxidation products generated in the OFR.<sup>2</sup> At  $\text{OH}_{\text{exp}} \geq 4$  days, the SOA concentration started to decrease due to heterogeneous oxidation-induced OA fragmentation.<sup>14</sup> Ammonium and nitrate aerosol enhancements of up to 0.8 and  $2.7 \mu\text{g m}^{-3}$  were observed at OH exposure ~1 equiv day followed by lower enhancements at higher  $\text{OH}_{\text{exp}}$ . This enhancement in secondary ammonium nitrate aerosol in OFR was mainly contributed by the reaction  $\text{NO}_2 + \text{OH} \rightarrow \text{HNO}_3$  followed by  $\text{NH}_3 + \text{HNO}_3 \rightarrow \text{NH}_4\text{NO}_3$ .<sup>22,25</sup> These inorganic nitrate formation in OFR were also supported by the similar  $\text{NO}_2^+/\text{NO}^+$  ratio from enhanced nitrate (0.35–0.38) compared to that from pure inorganic  $\text{NH}_4\text{NO}_3$  calibration aerosols (~0.37) and more neutralized aerosols at higher  $\text{OH}_{\text{exp}}$  (SI Figure S17). The reason we did not see organic nitrate influences to  $\text{NO}_2^+/\text{NO}^+$  ratio is likely due to the low contribution of organic nitrate concentration from  $\text{RO}_2 + \text{NO}$  pathways to the  $\text{NO}_2^+/\text{NO}^+$  ratio (<6%) compared to abundant ammonium nitrate formation in OFR.

Figure 3b compares the SOA formation potential of ambient air in Guangzhou with results obtained from previous OFR-based field studies in urban areas. To account for different dilution levels among the different studies, SOA mass concentrations were normalized to background-corrected CO levels ( $\Delta\text{CO}$ ).<sup>78</sup> This analysis assumes CO is a conserved tracer that is coemitted with reactive anthropogenic SOA precursors. Overall,  $\Delta\text{OA}/\Delta\text{CO}$  increases and then decreases as a function of  $\text{OH}_{\text{exp}}$ , with maximum  $\Delta\text{OA}/\Delta\text{CO}$  values observed between 1 and 4 equiv days (Figure 3b) of OH exposure equivalent time. These results suggest qualitatively similar SOA formation pathways are accessed via OH exposure across different urban studies.

For the absolute mass concentrations formed in OFR (accounting for direct effects of dilution), as shown in Figure 3b the  $\Delta\text{OA}/\Delta\text{CO}$  reported from near-source roadside and tunnel studies was generally higher than at urban background sites in Guangzhou, Los Angeles (LA) and Beijing, highlighting the potentially important influences of emission composition and secondary effects of atmospheric dilution on the measured SOA formation potential. Across the urban background sites,  $\Delta\text{OA}/\Delta\text{CO}$  values obtained in Guangzhou were higher than in LA and Beijing. We note that overall a similar VOC composition mix was measured in Guangzhou and LA, and that concentrations of those VOCs were approximately 1.7 times higher in Guangzhou than in LA (SI Figure S18), which is similar to the  $\Delta\text{OA}/\Delta\text{CO}$  ratio (1.7) between these two cities, yielding a similar VOCs normalized SOA formation potential ( $1.5 \mu\text{g m}^{-3} \text{ ppb}^{-1}$ ).

The OFR data can provide a unique opportunity for investigating the OA evolution from urban plumes since urban emission-dominated air masses would be difficult to distinguish after several days of aging due to the physical dilution and mixing.<sup>22</sup> In an attempt to use  $\Delta\text{OA}/\Delta\text{CO}$  values observed in the OFR to constrain ambient OA/ $\Delta\text{CO}$  values downwind of Guangzhou, we fit eq 1 to ambient and OFR OA/ $\Delta\text{CO}$  as described in<sup>22,80</sup>

$$\frac{\text{OA}}{\Delta\text{CO}} = \left\{ \frac{\text{POA} + \text{BGSOA}}{\Delta\text{CO}} + \frac{\text{VOC}^*}{\Delta\text{CO}} [1 - e^{(-\frac{t}{\tau})}] \right\} \quad (1)$$

Where OA is the sum of ambient OA plus OFR formed OA;  $(\text{POA} + \text{BGSOA})/\Delta\text{CO}$  is the primary OA plus regional background SOA, constrained at  $37.4 \mu\text{g m}^{-3} \text{ ppm}^{-1}$  based on the source apportionment results from the direct AMS measurement in this study, which can be found in details in Chen et al.<sup>50</sup>  $t$  is the OH equivalent photochemical age assuming an OH concentration of  $1.5 \times 10^6 \text{ molecules cm}^{-3}$  for intercomparability with other studies.<sup>79</sup> Note that the value of  $t$  here does not apply to the actual ambient SOA formation.  $\text{VOC}^*/\Delta\text{CO}$  is the primary emission ratio, that is, normalized primary VOC precursor concentration at photochemical age = 0 and  $\tau$  is the time scale for urban SOA formation. We calculate a maximum  $\text{VOC}^*/\Delta\text{CO} = 45 \pm 1.6 \mu\text{g m}^{-3} \text{ ppm}^{-1}$  and  $t = 0.4 \pm 0.1$  days in Guangzhou compared to  $\text{VOC}^*/\Delta\text{CO} = 56 \pm 1.6 \mu\text{g m}^{-3}$  and  $t = 0.3 \pm 0.1$  days in LA (Figure 3c). The OFR OA/ $\Delta\text{CO}$  line lies at the lower range of the updated SOA SIMPLE model results constrained based on ambient SOA measurement,<sup>17</sup> suggesting the updated SIMPLE model slightly overestimates the average  $\text{VOC}^*/\Delta\text{CO}$  in this study ( $73 \pm 24 \mu\text{g m}^{-3} \text{ ppm}^{-1}$ ), however, is still within the uncertainty range. Because we did not extend OA/ $\Delta\text{CO}$  variation beyond  $\text{OH}_{\text{exp}} = 10$  equiv days, the lifetime of OA

mass loss due to heterogeneous oxidation at higher  $\text{OH}_{\text{exp}}$  is not constrained by our measurements.

Figure 3d shows the diurnal variation of the maximum observed SOA enhancement in the OFR (Figure 3d). Higher SOA formation in the nighttime than daytime was observed, which is consistent with higher mixing ratios of total anthropogenic VOC precursors such as aromatics and long-chain alkanes in the nighttime (Figure 3d). This enhanced nighttime SOA formation in OFR has also been found in the other OFR field studies no matter in urban<sup>22,26</sup> or forest environments.<sup>23,24</sup> The enhanced SOA formation during night due to OH oxidation indicate larger SOA formation potential from precursors at night.

**3.3. Comparison between Measured and Predicted SOA Formation in OFR.** Figure 4 shows the study-average SOA enhancement of  $7.7 \mu\text{g m}^{-3}$  measured in the OFR (“formed SOA in OFR” bar) following  $\sim 5$  equiv days of OH exposure, and the SOA concentrations calculated from the measured consumption of  $C_8-C_{20}$  linear alkanes, mono- and poly-aromatic hydrocarbons, isoprene, and monoterpenes; Here we assume SOA fragmentation is minor at lower  $\text{OH}_{\text{exp}}$ .<sup>22,29</sup>

Depending on the parametrization that is applied, oxidation of these measured precursors explains  $\sim 51\text{--}73\%$  of the observed SOA in OFR when low- $\text{NO}_x$  SOA yield values are applied, versus  $26\text{--}58\%$  if high- $\text{NO}_x$  SOA yield values are assumed. The vapor wall-loss-corrected SOA yield parametrization from Ma et al.<sup>38</sup> serves as the upper limit estimate of SOA contribution from these precursors in all cases.

For comparison, the SOA estimation based on the ambient VOC oxidation using a time-resolved approach by considering OH photooxidation from Wang et al.<sup>81</sup> was also shown here (“Esti. SOA fr. VOCs” bar). In this method, the primary emission ratio of ambient VOC species versus CO was estimated when ambient photochemical age was zero. Photochemical age (0–0.5 days here) was calculated from  $m + p$ -xylene to ethylbenzene based on their different reaction rates with OH radicals.<sup>82</sup> The composition of ambient VOCs from primary emissions and observations on-site are shown in Figure 4a,b, respectively. The consumption of VOCs in ambient air was calculated based on their absolute concentration differences. The measured ambient SOA (“meas. amb SOA” bar) is estimated as the sum of the oxygenated OA factors (72% of OA) from the AMS ambient OA source apportionment results.

The Wang et al. method accounts for 26% of the observed ambient SOA formation if high  $\text{NO}_x$  laboratory SOA yield values are applied (Figure 4c), which is in agreement with the  $\sim 25\%$  fractional contribution of measured precursors to SOA enhancement observed in the OFR when the same SOA yield parametrization used by Wang et al. (2020) is applied here. We also investigated the photochemical age influences on SOA closure estimation since the ambient photochemical age (0–0.5 days) in this study is less than that from OFR (<5 days). SI Figure S21 shows the variation of the ratio of measured SOA vs estimated SOA in OFR at different photochemical age categories (<5 days) is within 20–30%, suggesting a small impact of photochemical age on SOA closure estimation. The ambient estimation represents the SOA formation from emission to the current observation site, while the SOA formation in OFR more resembles the plume oxidation in the later aging process. The similarity of SOA estimation results between ambient and OFR data sets supports the useful and

representative of OFR for investigating ambient SOA formations.

Across all cases that were studied, we estimate that OH oxidation of C<sub>8</sub>–C<sub>20</sub> linear alkanes contributed less SOA than single-ring aromatic VOCs. Contribution from cyclic alkanes were not constrained by our measurements, but may contribute a factor of ~1.3 higher SOA formation than linear alkanes that are coemitted from gasoline vehicles.<sup>83</sup> The updated emission inventory shows that ambient S/IVOCs in Guangzhou was mainly contributed by vehicle emissions (45%) and industry (38%).<sup>84</sup> A recent local tunnel study in Guangzhou suggested the ambient IVOCS from vehicle emission was dominated by gasoline vehicles (80%).<sup>85</sup> If we assume that ambient cyclic and linear alkane concentrations in Guangzhou are present in similar ratios as emitted by gasoline vehicles, then the total SOA contribution from linear and cyclic alkanes increases from 8 to 20% (linear only) to 17.5–46%. The updated IVOC contribution to SOA is comparable to the traditional VOCs (13–68%) when different SOA yields were applied, as shown in Figure 4c.

The inability of ambient OFR-based studies to apportion all the observed SOA formation to the OH oxidation of known precursors has been observed in both urban<sup>27,86</sup> and forest source regions.<sup>23,24</sup> The typical explanation attributed to this underestimation is the oxidation of unmeasured S/IVOCs,<sup>11,37,40</sup> which may include: (i) early generation oxidation products of VOCs in ambient air that are further oxidized in the OFR to generate additional SOA. (ii) Primary S/IVOCs, including newly identified volatile chemical products (VCP),<sup>12</sup> that can be important SOA precursors in urban environments.<sup>17,27</sup>

Although SVOCs were not measured here, Akherati et al.<sup>42</sup> used POA to constrain S/IVOC emissions and modeled SVOCs can contribute 20% (low NO<sub>x</sub> condition) and 95% (high NO<sub>x</sub> condition) of IVOC-derived SOA production in southern California. Since similar VOC-normalized SOA potential was observed between Guangzhou and Los Angeles, these estimated SOA ratios between SVOCs and IVOCs might also be applicable in this study. If such parametrization is used, the total SVOCs can contribute 4–10% fractions of total SOA formed in OFR at low NO<sub>x</sub> chemical regimes and 22–33% in high NO<sub>x</sub> chemical regimes, as shown in Figure 4c. Note that results are obtained based on a very simple ratio between modeled SVOC-SOA vs IVOC-SOA results, which might result in large uncertainty on the SVOC-SOA estimation in OFR here.

The total S/IVOC contribution generally contributes more than traditional VOCs under high NO<sub>x</sub> condition, however varied under low NO<sub>x</sub> condition. In total, when the Ma parameters are applied, the observed SOA can be fully explained from the measured VOCs/IVOCs plus estimated SOA from unmeasured S/IVOCs (e.g., cyclic alkanes) under high NO<sub>x</sub> condition, and Tsimpidi et al.<sup>87</sup> parametrization get closest estimation (92%) for low NO<sub>x</sub> conditions. In other parametrizations, 75–90% (low NO<sub>x</sub>) and 64–71% (high NO<sub>x</sub>) of SOA mass can be explained signifying the important S/IVOC contribution to ambient SOA formation.

Although unmeasured S/IVOC species cannot be directly quantified from our measurements, the measured/missed SOA shows better temporal correlation with VOCs of styrene, monoterpene, and C<sub>9</sub> aromatics which have high k<sub>OH</sub> of 2–6 × 10<sup>-11</sup> s<sup>-1</sup> molecules cm<sup>-3</sup>, as shown in SI Figure S22. This is similar to the results from Los Angeles, where Ortega et al.<sup>22</sup>

suggests species including S/IVOC with a similar source footprint and lifetime as C<sub>9</sub> aromatic produce most of the urban SOA based on the better correlation of formed SOA in OFR vs C<sub>9</sub> aromatic in LA study. This conclusion might also be applicable to our study here. Note that the monoterpenes measured in our study are probably dominated by the emission of anthropogenic sources, for example, fragranced VCP,<sup>88,89</sup> as good correlations between monoterpene and anthropogenic-originated C<sub>8</sub> aromatic species, as well as with CO were observed (SI Figure S23).<sup>50</sup>

#### 4. IMPLICATION OF THIS STUDY

An in situ OFR was used to investigate the OVOC and SOA formation from OH oxidation of gas-phase precursors present in urban plumes in Guangzhou, China. The greatly enhanced OVOC concentrations following OH exposure in the OFR signify the importance of gas-phase oxidation reactions. Maximum SOA formation potential was observed at a photochemical age of ~2 equiv days of atmospheric OH exposure in this study, compared to 1–4 equiv days' OH exposure in other urban OFR studies. We can explain 52–75% of observed SOA formed under low NO<sub>x</sub> conditions and 25–60% of SOA under high NO<sub>x</sub> conditions from precursors whose consumption in the OFR was directly measured. When SOA contributed by unexplained S/IVOCs was further estimated, 75%–100% formed SOA in OFR can be explained, emphasizing the important contribution from ambient S/IVOC species to SOA. Investigating SOA formation under an expanded set of variable and high-NO<sub>x</sub> OFR photochemical conditions using methods described in Lambe et al.<sup>90,91</sup> and Peng et al.<sup>92</sup> will be performed in future studies.

#### ASSOCIATED CONTENT

##### Supporting Information

The Supporting Information is available free of charge at <https://pubs.acs.org/doi/10.1021/acs.est.1c03155>.

Determination of OH exposure in the OFR (Text S1); Mass concentrations and measurement techniques of aerosol and gas phase species (Table S1); The chemical formula, structural formula and corresponding detection instruments of the VOCs (Table S2); References for different SOA yield parameters (Table S3); Detailed information on the OFR calibration experiments (Table S4); Parameters for OH exposure estimation equation (Table S5); Location of observation site (Figure S1); Schematic setup for OFR in the field and laboratory studies (Figure S2); Measured temperature and relative humidity in OFR and ambient air (Figure S3); Comparison of total aerosol measured by the AMS and SMPS (Figure S4); Mass size distribution in OFR and ambient air (Figure S5); Fractional fate of LVOC as a function of photochemical age (Figure S6); Speciated aerosol mass loss in OFR (Figure S7); Nitrate and chloride mass loss in OFR as a function of RH and Temperature (Figure S8); RO<sub>2</sub> reaction pathway (Figure S9); Measured residence time distribution of OFR (Figure S10); OH exposure experiment figures (Figure S11–16); Categorized ions measured by the CIMS in ambient air and OFR (Figure S17); Time series of main aerosol components and typical VOC species in ambient air and OFR (Figure S18); Molar ratio of measured ammonium vs predicted ammonium

(Figure S19); Formed SOA concentration as a function of photochemical age in OFR(Figure S21), and other supplementary figures (PDF)

## AUTHOR INFORMATION

### Corresponding Authors

**Weiwei Hu** – State Key Laboratory of Organic Geochemistry, Guangzhou Institute of Geochemistry, Chinese Academy of Sciences, Guangzhou, Guangdong 510640, China; CAS Center for Excellence in Deep Earth Science, Guangzhou, Guangdong 510640, China; Guangdong-Hong Kong-Macao, Joint Laboratory for Environmental Pollution and Control, Guangzhou Institute of Geochemistry, Chinese Academy of Science, Guangzhou, Guangdong 510640, China; Guangdong Provincial Key Laboratory of Environmental Protection and Resources Utilization, Chinese Academy of Science, Guangzhou, Guangdong 510640, China; [orcid.org/0000-0002-3485-6304](https://orcid.org/0000-0002-3485-6304); Email: [weiweihu@gig.ac.cn](mailto:weiweihu@gig.ac.cn)

**Xinming Wang** – State Key Laboratory of Organic Geochemistry, Guangzhou Institute of Geochemistry, Chinese Academy of Sciences, Guangzhou, Guangdong 510640, China; CAS Center for Excellence in Deep Earth Science, Guangzhou, Guangdong 510640, China; Guangdong-Hong Kong-Macao, Joint Laboratory for Environmental Pollution and Control, Guangzhou Institute of Geochemistry, Chinese Academy of Science, Guangzhou, Guangdong 510640, China; Guangdong Provincial Key Laboratory of Environmental Protection and Resources Utilization, Chinese Academy of Science, Guangzhou, Guangdong 510640, China; [orcid.org/0000-0002-1982-0928](https://orcid.org/0000-0002-1982-0928); Email: [wangxm@gig.ac.cn](mailto:wangxm@gig.ac.cn)

### Authors

**Huaishan Zhou** – State Key Laboratory of Organic Geochemistry, Guangzhou Institute of Geochemistry, Chinese Academy of Sciences, Guangzhou, Guangdong 510640, China; University of Chinese Academy of Sciences, Beijing 100049, China

**Wei Chen** – State Key Laboratory of Organic Geochemistry, Guangzhou Institute of Geochemistry, Chinese Academy of Sciences, Guangzhou, Guangdong 510640, China; University of Chinese Academy of Sciences, Beijing 100049, China

**Yuqing Ye** – State Key Laboratory of Organic Geochemistry, Guangzhou Institute of Geochemistry, Chinese Academy of Sciences, Guangzhou, Guangdong 510640, China

**Tianle Pan** – State Key Laboratory of Organic Geochemistry, Guangzhou Institute of Geochemistry, Chinese Academy of Sciences, Guangzhou, Guangdong 510640, China; University of Chinese Academy of Sciences, Beijing 100049, China

**Yingkun Wang** – State Key Laboratory of Organic Geochemistry, Guangzhou Institute of Geochemistry, Chinese Academy of Sciences, Guangzhou, Guangdong 510640, China; University of Chinese Academy of Sciences, Beijing 100049, China

**Wei Song** – State Key Laboratory of Organic Geochemistry, Guangzhou Institute of Geochemistry, Chinese Academy of Sciences, Guangzhou, Guangdong 510640, China; CAS Center for Excellence in Deep Earth Science, Guangzhou, Guangdong 510640, China; Guangdong-Hong Kong-Macao, Joint Laboratory for Environmental Pollution and Control, Guangzhou Institute of Geochemistry, Chinese Academy of Science, Guangzhou, Guangdong 510640, China; Guangdong Provincial Key Laboratory of Environmental Protection and

Resources Utilization, Chinese Academy of Science, Guangzhou, Guangdong 510640, China

**Huina Zhang** – State Key Laboratory of Organic Geochemistry, Guangzhou Institute of Geochemistry, Chinese Academy of Sciences, Guangzhou, Guangdong 510640, China; University of Chinese Academy of Sciences, Beijing 100049, China

**Wei Deng** – State Key Laboratory of Organic Geochemistry, Guangzhou Institute of Geochemistry, Chinese Academy of Sciences, Guangzhou, Guangdong 510640, China; University of Chinese Academy of Sciences, Beijing 100049, China

**Ming Zhu** – State Key Laboratory of Organic Geochemistry, Guangzhou Institute of Geochemistry, Chinese Academy of Sciences, Guangzhou, Guangdong 510640, China; University of Chinese Academy of Sciences, Beijing 100049, China; [orcid.org/0000-0003-2288-6271](https://orcid.org/0000-0003-2288-6271)

**Chaomin Wang** – Institute for Environmental and Climate Research, Jinan University, Guangzhou, Guangdong 511443, China

**Caihong Wu** – Institute for Environmental and Climate Research, Jinan University, Guangzhou, Guangdong 511443, China

**Chenshuo Ye** – Institute for Environmental and Climate Research, Jinan University, Guangzhou, Guangdong 511443, China

**Zelong Wang** – Institute for Environmental and Climate Research, Jinan University, Guangzhou, Guangdong 511443, China

**Bin Yuan** – Institute for Environmental and Climate Research, Jinan University, Guangzhou, Guangdong 511443, China; [orcid.org/0000-0003-3041-0329](https://orcid.org/0000-0003-3041-0329)

**Shan Huang** – Institute for Environmental and Climate Research, Jinan University, Guangzhou, Guangdong 511443, China

**Min Shao** – Institute for Environmental and Climate Research, Jinan University, Guangzhou, Guangdong 511443, China

**Zhe Peng** – Cooperative Institute for Research in the Environmental Sciences (CIRES), University of Colorado at Boulder, Boulder, Colorado 80309, United States; Department of Chemistry, University of Colorado at Boulder, Boulder, Colorado 80309, United States

**Douglas A. Day** – Cooperative Institute for Research in the Environmental Sciences (CIRES), University of Colorado at Boulder, Boulder, Colorado 80309, United States; Department of Chemistry, University of Colorado at Boulder, Boulder, Colorado 80309, United States

**Pedro Campuzano-Jost** – Cooperative Institute for Research in the Environmental Sciences (CIRES), University of Colorado at Boulder, Boulder, Colorado 80309, United States; Department of Chemistry, University of Colorado at Boulder, Boulder, Colorado 80309, United States; [orcid.org/0000-0003-3930-010X](https://orcid.org/0000-0003-3930-010X)

**Andrew T. Lambe** – Aerodyne Research Inc., Billerica, Massachusetts 01821, United States; [orcid.org/0000-0003-3031-701X](https://orcid.org/0000-0003-3031-701X)

**Douglas R Worsnop** – Aerodyne Research Inc., Billerica, Massachusetts 01821, United States

**Jose L. Jimenez** – Cooperative Institute for Research in the Environmental Sciences (CIRES), University of Colorado at Boulder, Boulder, Colorado 80309, United States; Department of Chemistry, University of Colorado at Boulder, Boulder, Colorado 80309, United States; [orcid.org/0000-0001-6203-1847](https://orcid.org/0000-0001-6203-1847)

Complete contact information is available at:  
<https://pubs.acs.org/10.1021/acs.est.1c03155>

## Notes

The authors declare no competing financial interest.

## ACKNOWLEDGMENTS

This work was supported by National Natural Science Foundation of China (Grant No. 41875156), Natural Science Foundation of Guangdong Province (Grant No. 2019A1515011153), Guangdong Pearl River Talents Program (2019QN01L948), Guangdong Foundation for Program of Science and Technology Research (Grant No. 2020B1212060053), Guangdong Foundation for Program of Science and Technology Research (Grant No. 2020B1212060053, 2017B030314057), State Key Laboratory of Organic Geochemistry, GIGCAS (SKLOG2020-5, SKLOG2020-6). Bin Yuan was supported by the National Key R&D Plan of China (grant No. 2019YFE0106300), the National Natural Science Foundation of China (grant No. 41877302), Guangdong Natural Science Funds for Distinguished Young Scholar (Grant No. 2018B030306037), and Guangdong Innovative and Entrepreneurial Research Team Program (Grant No. 2016ZT06N263). Z.P., D.D., P.C.J., and J.L.J were supported by the U.S. National Science Foundation (Grant No. NSF AGS-1822664).

## REFERENCES

- (1) Zhang, Q.; Jimenez, J. L.; Canagaratna, M. R.; Allan, J. D.; Coe, H.; Ulbrich, I.; Alfarra, M. R.; Takami, A.; Middlebrook, A. M.; Sun, Y. L.; Dzepina, K.; Dunlea, E.; Docherty, K.; DeCarlo, P. F.; Salcedo, D.; Onasch, T.; Jayne, J. T.; Miyoshi, T.; Shimono, A.; Hatakeyama, S.; Takegawa, N.; Kondo, Y.; Schneider, J.; Drewnick, F.; Borrmann, S.; Weimer, S.; Demerjian, K.; Williams, P.; Bower, K.; Bahreini, R.; Cottrell, L.; Griffin, R. J.; Rautiainen, J.; Sun, J. Y.; Zhang, Y. M.; Worsnop, D. R. Ubiquity and dominance of oxygenated species in organic aerosols in anthropogenically-influenced Northern Hemisphere midlatitudes. *Geophys. Res. Lett.* **2007**, *34* (13), L13801 and references therein..
- (2) Jimenez, J. L.; Canagaratna, M. R.; Donahue, N. M.; Prevot, A. S. H.; Zhang, Q.; Kroll, J. H.; DeCarlo, P. F.; Allan, J. D.; Coe, H.; Ng, N. L.; Aiken, A. C.; Docherty, K. S.; Ulbrich, I. M.; Grieshop, A. P.; Robinson, A. L.; Duplissy, J.; Smith, J. D.; Wilson, K. R.; Lanz, V. A.; Hueglin, C.; Sun, Y. L.; Tian, J.; Laaksonen, A.; Raatikainen, T.; Rautiainen, J.; Vaattovaara, P.; Ehn, M.; Kulmala, M.; Tomlinson, J. M.; Collins, D. R.; Cubison, M. J.; Dunlea, E. J.; Huffman, J. A.; Onasch, T. B.; Alfarra, M. R.; Williams, P. I.; Bower, K.; Kondo, Y.; Schneider, J.; Drewnick, F.; Borrmann, S.; Weimer, S.; Demerjian, K.; Salcedo, D.; Cottrell, L.; Griffin, R.; Takami, A.; Miyoshi, T.; Hatakeyama, S.; Shimono, A.; Sun, J. Y.; Zhang, Y. M.; Dzepina, K.; Kimmel, J. R.; Sueper, D.; Jayne, J. T.; Herndon, S. C.; Trimborn, A. M.; Williams, L. R.; Wood, E. C.; Middlebrook, A. M.; Kolb, C. E.; Baltensperger, U.; Worsnop, D. R. Evolution of Organic Aerosols in the Atmosphere. *Science* **2009**, *326* (5959), 1525–1529 and references therein.
- (3) Hodzic, A.; Campuzano-Jost, P.; Bian, H.; Chin, M.; Colarco, P. R.; Day, D. A.; Froyd, K. D.; Heinold, B.; Jo, D. S.; Katich, J. M.; Kodros, J. K.; Nault, B. A.; Pierce, J. R.; Ray, E.; Schacht, J.; Schill, G. P.; Schroder, J. C.; Schwarz, J. P.; Sueper, D. T.; Tegen, I.; Tilmes, S.; Tsigaridis, K.; Yu, P.; Jimenez, J. L. Characterization of organic aerosol across the global remote troposphere: a comparison of ATom measurements and global chemistry models. *Atmos. Chem. Phys.* **2020**, *20* (8), 4607–4635.
- (4) IPCC. *Intergovernmental Panel on Climate Change (IPCC): Climate Change: The Scientific Basis*; Cambridge University Press: UK, 2017.
- (5) Shrivastava, M.; Cappa, C. D.; Fan, J.; Goldstein, A. H.; Guenther, A. B.; Jimenez, J. L.; Kuang, C.; Laskin, A.; Martin, S. T.; Ng, N. L.; Petaja, T.; Pierce, J. R.; Rasch, P. J.; Roldin, P.; Seinfeld, J. H.; Shilling, J.; Smith, J. N.; Thornton, J. A.; Volkamer, R.; Wang, J.; Worsnop, D. R.; Zaveri, R. A.; Zelenyuk, A.; Zhang, Q. Recent advances in understanding secondary organic aerosol: Implications for global climate forcing. *Rev. Geophys.* **2017**, *55* (2), S09–S59.
- (6) Mauderly, J. L.; Chow, J. C. Health Effects of Organic Aerosols. *Inhalation Toxicol.* **2008**, *20* (3), 257–288.
- (7) Shiraiwa, M.; Ueda, K.; Pozzer, A.; Lammel, G.; Kampf, C. J.; Fushimi, A.; Enami, S.; Arangio, A. M.; Fröhlich-Nowoisky, J.; Fujitani, Y.; Furuyama, A.; Lakey, P. S. J.; Lelieveld, J.; Lucas, K.; Morino, Y.; Pöschl, U.; Takahama, S.; Takami, A.; Tong, H.; Weber, B.; Yoshino, A.; Sato, K. Aerosol Health Effects from Molecular to Global Scales. *Environ. Sci. Technol.* **2017**, *51* (23), 13545–13567.
- (8) Hallquist, M.; Wenger, J. C.; Baltensperger, U.; Rudich, Y.; Simpson, D.; Claeys, M.; Dommen, J.; Donahue, N. M.; George, C.; Goldstein, A. H.; Hamilton, J. F.; Herrmann, H.; Hoffmann, T.; Iinuma, Y.; Jang, M.; Jenkin, M. E.; Jimenez, J. L.; Kiendler-Scharr, A.; Maenhaut, W.; McFiggans, G.; Mentel, T. F.; Monod, A.; Prevot, A. S. H.; Seinfeld, J. H.; Surratt, J. D.; Szmigielski, R.; Wildt, J. The formation, properties and impact of secondary organic aerosols: current and emerging issues. *Atmos. Chem. Phys.* **2009**, *9* (14), 5155–5236.
- (9) Donahue, N. M.; Henry, K. M.; Mentel, T. F.; Kiendler-Scharr, A.; Spindler, C.; Bohn, B.; Brauers, T.; Dorn, H. P.; Fuchs, H.; Tillmann, R.; Wahner, A.; Saathoff, H.; Naumann, K.-H.; Möhler, O.; Leisner, T.; Müller, L.; Reinig, M.-C.; Hoffmann, T.; Salo, K.; Hallquist, M.; Frosch, M.; Bilde, M.; Tritscher, T.; Barmet, P.; Praplan, A. P.; DeCarlo, P. F.; Dommen, J.; Prévôt, A. S. H.; Baltensperger, U. Aging of biogenic secondary organic aerosol via gas-phase OH radical reactions. *Proc. Natl. Acad. Sci. U. S. A.* **2012**, *109* (34), 13503–13508.
- (10) Ziemann, P. J.; Atkinson, R. Kinetics, products, and mechanisms of secondary organic aerosol formation. *Chem. Soc. Rev.* **2012**, *41* (19), 6582–6605.
- (11) Robinson, A. L.; Donahue, N. M.; Shrivastava, M. K.; Weitkamp, E. A.; Sage, A. M.; Grieshop, A. P.; Lane, T. E.; Pierce, J. R.; Pandis, S. N. Rethinking organic aerosols: Semivolatile emissions and photochemical aging. *Science* **2007**, *315* (5816), 1259–1262.
- (12) McDonald, B. C.; de Gouw, J. A.; Gilman, J. B.; Jathar, S. H.; Akherati, A.; Cappa, C. D.; Jimenez, J. L.; Lee-Taylor, J.; Hayes, P. L.; McKeen, S. A.; Cui, Y. Y.; Kim, S.-W.; Gentner, D. R.; Isaacman-VanWertz, G.; Goldstein, A. H.; Harley, R. A.; Frost, G. J.; Roberts, J. M.; Ryerson, T. B.; Trainer, M. Volatile chemical products emerging as largest petrochemical source of urban organic emissions. *Science* **2018**, *359* (6377), 760–764.
- (13) Ervens, B.; Turpin, B. J.; Weber, R. J. Secondary organic aerosol formation in cloud droplets and aqueous particles (aqSOA): a review of laboratory, field and model studies. *Atmos. Chem. Phys.* **2011**, *11* (21), 11069–11102.
- (14) Kroll, J. H.; Lim, C. Y.; Kessler, S. H.; Wilson, K. R. Heterogeneous Oxidation of Atmospheric Organic Aerosol: Kinetics of Changes to the Amount and Oxidation State of Particle-Phase Organic Carbon. *J. Phys. Chem. A* **2015**, *119* (44), 10767–10783.
- (15) Tsigaridis, K.; Daskalakis, N.; Kanakidou, M.; Adams, P. J.; Artaxo, P.; Bahadur, R.; Balkanski, Y.; Bauer, S. E.; Bellouin, N.; Benedetti, A.; Bergman, T.; Berntsen, T. K.; Beukes, J. P.; Bian, H.; Carslaw, K. S.; Chin, M.; Curci, G.; Diehl, T.; Easter, R. C.; Ghan, S. J.; Gong, S. L.; Hodzic, A.; Hoyle, C. R.; Iversen, T.; Jathar, S.; Jimenez, J. L.; Kaiser, J. W.; Kirkevåg, A.; Koch, D.; Kokkola, H.; Lee, Y. H.; Lin, G.; Liu, X.; Luo, G.; Ma, X.; Mann, G. W.; Mihalopoulos, N.; Morcrette, J. J.; Müller, J. F.; Myhre, G.; Myrookefalitakis, S.; Ng, N. L.; O'Donnell, D.; Penner, J. E.; Pozzoli, L.; Pringle, K. J.; Russell, L. M.; Schulz, M.; Scire, J.; Seland, I.; Shindell, D. T.; Sillman, S.; Skeie, R. B.; Spracklen, D.; Stavrakou, T.; Steenrod, S. D.; Takemura, T.; Tiitta, P.; Tilmes, S.; Tost, H.; van Noije, T.; van Zyl, P. G.; von Salzen, K.; Yu, F.; Wang, Z.; Zaveri, R. A.; Zhang, H.; Zhang, K.;

- Zhang, Q.; Zhang, X. The AeroCom evaluation and intercomparison of organic aerosol in global models. *Atmos. Chem. Phys.* **2014**, *14* (19), 10845–10895.
- (16) Volkamer, R.; Martini, F. S.; Molina, L. T.; Salcedo, D.; Jimenez, J. L.; Molina, M. J. A missing sink for gas-phase glyoxal in Mexico City: Formation of secondary organic aerosol. *Geophys. Res. Lett.* **2007**, *34* (19), DOI: 10.1029/2007GL030752.
- (17) Nault, B. A.; Jo, D. S.; McDonald, B. C.; Campuzano-Jost, P.; Day, D. A.; Hu, W.; Schroder, J. C.; Allan, J.; Blake, D. R.; Canagaratna, M. R.; Coe, H.; Coggon, M. M.; DeCarlo, P. F.; Diskin, G. S.; Dunmore, R.; Flocke, F.; Fried, A.; Gilman, J. B.; Gkatzelis, G.; Hamilton, J. F.; Hanisco, T. F.; Hayes, P. L.; Henze, D. K.; Hodzic, A.; Hopkins, J.; Hu, M.; Huey, L. G.; Jobson, B. T.; Kuster, W. C.; Lewis, A.; Li, M.; Liao, J.; Nawaz, M. O.; Pollack, I. B.; Peischl, J.; Rappenglück, B.; Reeves, C. E.; Richter, D.; Roberts, J. M.; Ryerson, T. B.; Shao, M.; Sommers, J. M.; Walega, J.; Warneke, C.; Weibring, P.; Wolfe, G. M.; Young, D. E.; Yuan, B.; Zhang, Q.; de Gouw, J. A.; Jimenez, J. L. Anthropogenic Secondary Organic Aerosols Contribute Substantially to Air Pollution Mortality. *Atmos. Chem. Phys. Discuss.* **2020**, *2020*, 1–53, DOI: 10.5194/acp-21-11201-2021.
- (18) Kang, E.; Root, M. J.; Toohey, D. W.; Brune, W. H. Introducing the concept of Potential Aerosol Mass (PAM). *Atmos. Chem. Phys.* **2007**, *7* (22), 5727–5744.
- (19) Kang, E.; Toohey, D. W.; Brune, W. H. Dependence of SOA oxidation on organic aerosol mass concentration and OH exposure: experimental PAM chamber studies. *Atmos. Chem. Phys.* **2011**, *11* (4), 1837–1852.
- (20) Lambe, A. T.; Ahern, A. T.; Williams, L. R.; Slowik, J. G.; Wong, J. P. S.; Abbatt, J. P. D.; Brune, W. H.; Ng, N. L.; Wright, J. P.; Croasdale, D. R.; Worsnop, D. R.; Davidovits, P.; Onasch, T. B. Characterization of aerosol photooxidation flow reactors: heterogeneous oxidation, secondary organic aerosol formation and cloud condensation nuclei activity measurements. *Atmos. Meas. Tech.* **2011**, *4* (3), 445–461.
- (21) Li, J.; Liu, Q.; Li, Y.; Liu, T.; Huang, D.; Zheng, J.; Zhu, W.; Hu, M.; Wu, Y.; Lou, S.; Hallquist, M.; Hallquist, M.; Chan, C. K.; Canonaco, F.; Prévôt, A. S. H.; Fung, J. C. H.; Lau, A. K. H.; Yu, J. Z. Characterization of Aerosol Aging Potentials at Suburban Sites in Northern and Southern China Utilizing a Potential Aerosol Mass (Go:PAM) Reactor and an Aerosol Mass Spectrometer. *J. Geophys. Res.: Atmos.* **2019**, *124* (10), 5629–5649.
- (22) Ortega, A. M.; Hayes, P. L.; Peng, Z.; Palm, B. B.; Hu, W.; Day, D. A.; Li, R.; Cubison, M. J.; Brune, W. H.; Graus, M.; Warneke, C.; Gilman, J. B.; Kuster, W. C.; de Gouw, J.; Gutiérrez-Montes, C.; Jimenez, J. L. Real-time measurements of secondary organic aerosol formation and aging from ambient air in an oxidation flow reactor in the Los Angeles area. *Atmos. Chem. Phys.* **2016**, *16* (11), 7411–7433.
- (23) Palm, B. B.; Campuzano-Jost, P.; Ortega, A. M.; Day, D. A.; Kaser, L.; Jud, W.; Karl, T.; Hansel, A.; Hunter, J. F.; Cross, E. S.; Kroll, J. H.; Peng, Z.; Brune, W. H.; Jimenez, J. L. In situ secondary organic aerosol formation from ambient pine forest air using an oxidation flow reactor. *Atmos. Chem. Phys.* **2016**, *16* (5), 2943–2970.
- (24) Palm, B. B.; de Sá, S. S.; Day, D. A.; Campuzano-Jost, P.; Hu, W.; Seco, R.; Sjostedt, S. J.; Park, J. H.; Guenther, A. B.; Kim, S.; Brito, J.; Wurm, F.; Artaxo, P.; Thalman, R.; Wang, J.; Yee, L. D.; Wernis, R.; Isaacman-VanWertz, G.; Goldstein, A. H.; Liu, Y.; Springston, S. R.; Souza, R.; Newburn, M. K.; Alexander, M. L.; Martin, S. T.; Jimenez, J. L. Secondary organic aerosol formation from ambient air in an oxidation flow reactor in central Amazonia. *Atmos. Chem. Phys.* **2018**, *18* (1), 467–493.
- (25) Tkacik, D. S.; Lambe, A. T.; Jathar, S.; Li, X.; Presto, A. A.; Zhao, Y.; Blake, D.; Meinardi, S.; Jayne, J. T.; Croteau, P. L.; Robinson, A. L. Secondary Organic Aerosol Formation from in-Use Motor Vehicle Emissions Using a Potential Aerosol Mass Reactor. *Environ. Sci. Technol.* **2014**, *48* (19), 11235–11242.
- (26) Saha, P. K.; Reece, S. M.; Grieshop, A. P., Seasonally Varying Secondary Organic Aerosol Formation From In-Situ Oxidation of Near-Highway Air. *Environ. Sci. Technol.* **2018**, 527192.
- (27) Shah, R. U.; Coggon, M. M.; Gkatzelis, G. I.; McDonald, B. C.; Tasoglou, A.; Huber, H.; Gilman, J.; Warneke, C.; Robinson, A. L.; Presto, A. A. Urban Oxidation Flow Reactor Measurements Reveal Significant Secondary Organic Aerosol Contributions from Volatile Emissions of Emerging Importance. *Environ. Sci. Technol.* **2020**, 54714.
- (28) Lambe, A. T.; Onasch, T. B.; Croasdale, D. R.; Wright, J. P.; Martin, A. T.; Franklin, J. P.; Massoli, P.; Kroll, J. H.; Canagaratna, M. R.; Brune, W. H.; Worsnop, D. R.; Davidovits, P. Transitions from Functionalization to Fragmentation Reactions of Laboratory Secondary Organic Aerosol (SOA) Generated from the OH Oxidation of Alkane Precursors. *Environ. Sci. Technol.* **2012**, *46* (10), 5430–5437.
- (29) Hu, W.; Palm, B. B.; Day, D. A.; Campuzano-Jost, P.; Krechmer, J. E.; Peng, Z.; de Sá, S. S.; Martin, S. T.; Alexander, M. L.; Baumann, K.; Hacker, L.; Kiendler-Scharr, A.; Koss, A. R.; de Gouw, J. A.; Goldstein, A. H.; Seco, R.; Sjostedt, S. J.; Park, J. H.; Guenther, A. B.; Kim, S.; Canonaco, F.; Prévôt, A. S. H.; Brune, W. H.; Jimenez, J. L. Volatility and lifetime against OH heterogeneous reaction of ambient isoprene-epoxydiols-derived secondary organic aerosol (IEPOX-SOA). *Atmos. Chem. Phys.* **2016**, *16* (18), 11563–11580.
- (30) Palm, B. B.; Campuzano-Jost, P.; Day, D. A.; Ortega, A. M.; Fry, J. L.; Brown, S. S.; Zarzana, K. J.; Dube, W.; Wagner, N. L.; Draper, D. C.; Kaser, L.; Jud, W.; Karl, T.; Hansel, A.; Gutiérrez-Montes, C.; Jimenez, J. L. Secondary organic aerosol formation from in situ OH, O<sub>3</sub>, and NO<sub>3</sub> oxidation of ambient forest air in an oxidation flow reactor. *Atmos. Chem. Phys.* **2017**, *17* (8), 5331–5354.
- (31) Liu, J.; Chu, B.; Chen, T.; Liu, C.; Wang, L.; Bao, X.; He, H. Secondary Organic Aerosol Formation from Ambient Air at an Urban Site in Beijing: Effects of OH Exposure and Precursor Concentrations. *Environ. Sci. Technol.* **2018**, *52* (12), 6834–6841.
- (32) Liu, T.; Zhou, L.; Liu, Q.; Lee, B. P.; Yao, D.; Lu, H.; Lyu, X.; Guo, H.; Chan, C. K., Secondary Organic Aerosol Formation from Urban Roadside Air in Hong Kong. *Environ. Sci. Technol.* **2019**, 533001.
- (33) Liao, K.; Chen, Q.; Liu, Y.; Li, Y. J.; Lambe, A. T.; Zhu, T.; Huang, R.-J.; Zheng, Y.; Cheng, X.; Miao, R.; Huang, G.; Khuzestani, R. B.; Jia, T. Secondary Organic Aerosol Formation of Fleet Vehicle Emissions in China: Potential Seasonality of Spatial Distributions. *Environ. Sci. Technol.* **2021**, *55*, 7276–7286.
- (34) Nault, B. A.; Campuzano-Jost, P.; Day, D. A.; Schroder, J. C.; Anderson, B.; Beyersdorf, A. J.; Blake, D. R.; Brune, W. H.; Choi, Y.; Corr, C. A.; de Gouw, J. A.; Dibb, J.; DiGangi, J. P.; Diskin, G. S.; Fried, A.; Huey, L. G.; Kim, M. J.; Knote, C. J.; Lamb, K. D.; Lee, T.; Park, T.; Pusede, S. E.; Scheuer, E.; Thornhill, K. L.; Woo, J. H.; Jimenez, J. L. Secondary Organic Aerosol Production from Local Emissions Dominates the Organic Aerosol Budget over Seoul, South Korea, during KORUS-AQ. *Atmos. Chem. Phys.* **2018**, *18* (24), 17769–17800.
- (35) Tkacik, D. S.; Presto, A. A.; Donahue, N. M.; Robinson, A. L. Secondary Organic Aerosol Formation from Intermediate-Volatility Organic Compounds: Cyclic, Linear, and Branched Alkanes. *Environ. Sci. Technol.* **2012**, *46* (16), 8773–8781.
- (36) Li, K.; Liglio, J.; Lee, P.; Han, C.; Liu, Q.; Li, S. M. Secondary organic aerosol formation from  $\alpha$ -pinene, alkanes, and oil-sands-related precursors in a new oxidation flow reactor. *Atmos. Chem. Phys.* **2019**, *19* (15), 9715–9731.
- (37) Hunter, J. F.; Day, D. A.; Palm, B. B.; Yatavelli, R. L. N.; Chan, A. W. H.; Kaser, L.; Cappellin, L.; Hayes, P. L.; Cross, E. S.; Carrasquillo, A. J.; Campuzano-Jost, P.; Stark, H.; Zhao, Y.; Hohaus, T.; Smith, James N.; Hansel, A.; Karl, T.; Goldstein, A. H.; Guenther, A.; Worsnop, Douglas R.; Thornton, J. A.; Heald, C. L.; Jimenez, J. L.; Kroll, J. H. Comprehensive characterization of atmospheric organic carbon at a forested site. *Nat. Geosci.* **2017**, *10*, 748.
- (38) Ma, P. K.; Zhao, Y.; Robinson, A. L.; Worton, D. R.; Goldstein, A. H.; Ortega, A. M.; Jimenez, J. L.; Zotter, P.; Prévôt, A. S. H.; Szidat, S.; Hayes, P. L. Evaluating the impact of new observational constraints on P-S/IVOC emissions, multi-generation oxidation, and chamber wall losses on SOA modeling for Los Angeles, CA. *Atmos. Chem. Phys.* **2017**, *17* (15), 9237–9259.

- (39) Lu, Q.; Zhao, Y.; Robinson, A. L. Comprehensive organic emission profiles for gasoline, diesel, and gas-turbine engines including intermediate and semi-volatile organic compound emissions. *Atmos. Chem. Phys.* **2018**, *18* (23), 17637–17654.
- (40) Ma, N.; Zhao, C.; Tao, J.; Wu, Z.; Kecorius, S.; Wang, Z.; Grōš, J.; Liu, H.; Bian, Y.; Kuang, Y.; Teich, M.; Spindler, G.; Müller, K.; van Pinxteren, D.; Herrmann, H.; Hu, M.; Wiedensohler, A. Variation of CCN activity during new particle formation events in the North China Plain. *Atmos. Chem. Phys.* **2016**, *16* (13), 8593–8607.
- (41) Hodzic, A.; Jimenez, J. L. Modeling anthropogenically controlled secondary organic aerosols in a megacity: a simplified framework for global and climate models. *Geosci. Model Dev.* **2011**, *4* (4), 901–917.
- (42) Akherati, A.; Cappa, C. D.; Kleeman, M. J.; Docherty, K. S.; Jimenez, J. L.; Griffith, S. M.; Dusant, S.; Stevens, P. S.; Jathar, S. H. Simulating secondary organic aerosol in a regional air quality model using the statistical oxidation model -Part 3: Assessing the influence of semi-volatile and intermediate-volatility organic compounds and NO<sub>x</sub>. *Atmos. Chem. Phys.* **2019**, *19* (7), 4561–4594.
- (43) Jathar, S. H.; Woody, M.; Pye, H. O. T.; Baker, K. R.; Robinson, A. L. Chemical transport model simulations of organic aerosol in southern California: model evaluation and gasoline and diesel source contributions. *Atmos. Chem. Phys.* **2017**, *17* (6), 4305–4318.
- (44) Tsimpidi, A. P.; Karydis, V. A.; Zavala, M.; Lei, W.; Molina, L.; Ulbrich, I. M.; Jimenez, J. L.; Pandis, S. N. Evaluation of the volatility basis-set approach for the simulation of organic aerosol formation in the Mexico City metropolitan area. *Atmos. Chem. Phys.* **2010**, *10* (2), 525–546.
- (45) Wu, C.; Wang, C.; Wang, S.; Wang, W.; Yuan, B.; Qi, J.; Wang, B.; Wang, H.; Wang, C.; Song, W.; Wang, X.; Hu, W.; Lou, S.; Ye, C.; Peng, Y.; Wang, Z.; Huangfu, Y.; Xie, Y.; Zhu, M.; Zheng, J.; Wang, X.; Jiang, B.; Zhang, Z.; Shao, M. Measurement report: Important contributions of oxygenated compounds to emissions and chemistry of volatile organic compounds in urban air. *Atmos. Chem. Phys.* **2020**, *20* (23), 14769–14785.
- (46) Li, R.; Palm, B. B.; Ortega, A. M.; Hlywiak, J. A.; Hu, W.; Peng, Z.; Day, D. A.; Knote, C.; Brune, W. H.; de Gouw, J. A.; Jimenez, J. L. Modeling the Radical Chemistry in an Oxidation Flow Reactor: Radical Formation and Recycling, Sensitivities, and OH Exposure Estimation Equation. *J. Phys. Chem. A* **2015**, *119* (19), 4418–4432.
- (47) Peng, Z.; Day, D. A.; Ortega, A. M.; Palm, B. B.; Hu, W.; Stark, H.; Li, R.; Tsigaris, K.; Brune, W. H.; Jimenez, J. L. Non-OH chemistry in oxidation flow reactors for the study of atmospheric chemistry systematically examined by modeling. *Atmos. Chem. Phys.* **2016**, *16* (7), 4283–4305.
- (48) Peng, Z.; Day, D. A.; Stark, H.; Li, R.; Lee-Taylor, J.; Palm, B. B.; Brune, W. H.; Jimenez, J. L. HO<sub>x</sub> radical chemistry in oxidation flow reactors with low-pressure mercury lamps systematically examined by modeling. *Atmos. Meas. Tech.* **2015**, *8* (11), 4863–4890.
- (49) Deming, B. L.; Pagonis, D.; Liu, X.; Day, D. A.; Talukdar, R.; Krechmer, J. E.; de Gouw, J. A.; Jimenez, J. L.; Ziemann, P. J. Measurements of delays of gas-phase compounds in a wide variety of tubing materials due to gas-wall interactions. *Atmos. Meas. Tech.* **2019**, *12* (6), 3453–3461.
- (50) Chen, W.; Ye, Y.; Hu, W.; Zhou, H.; Pan, T.; Wang, Y.; Song, W.; Song, Q.; Ye, C.; Wang, C.; Wang, B.; Huang, S.; Yuan, B.; Zhu, M.; Lian, X.; Zhang, G.; Bi, X.; Jiang, F.; Liu, J.; Canonaco, F.; Prevot, A. S. H.; Shao, M.; Wang, X. Real-Time Characterization of Aerosol Compositions, Sources, and Aging Processes in Guangzhou During PRIDE-GBA 2018 Campaign. *J. Geophys. Res.: Atmos.* **2021**, *126* (16), No. e2021JD035114.
- (51) Peng, Z.; Jimenez, J. L., Radical chemistry in oxidation flow reactors for atmospheric chemistry research. *Chem. Soc. Rev.* **2020**, 492570.
- (52) Hu, W.; Campuzano-Jost, P.; Day, D. A.; Nault, B. A.; Park, T.; Lee, T.; Pajunoja, A.; Virtanen, A.; Croteau, P.; Canagaratna, M. R.; Jayne, J. T.; Worsnop, D. R.; Jimenez, J. L. Ambient Quantification and Size Distributions for Organic Aerosol in Aerosol Mass Spectrometers with the New Capture Vaporizer. *ACS Earth and Space Chemistry* **2020**, *4* (5), 676–689.
- (53) Canagaratna, M. R.; Jayne, J. T.; Jimenez, J. L.; Allan, J. D.; Alfarra, M. R.; Zhang, Q.; Onasch, T. B.; Drewnick, F.; Coe, H.; Middlebrook, A.; Delia, A.; Williams, L. R.; Trimborn, A. M.; Northway, M. J.; DeCarlo, P. F.; Kolb, C. E.; Davidovits, P.; Worsnop, D. R. Chemical and microphysical characterization of ambient aerosols with the aerodyne aerosol mass spectrometer. *Mass Spectrom. Rev.* **2007**, *26* (2), 185–222.
- (54) DeCarlo, P. F.; Kimmel, J. R.; Trimborn, A.; Northway, M. J.; Jayne, J. T.; Aiken, A. C.; Gonin, M.; Fuhrer, K.; Horvath, T.; Docherty, K. S.; Worsnop, D. R.; Jimenez, J. L. Field-deployable, high-resolution, time-of-flight aerosol mass spectrometer. *Anal. Chem.* **2006**, *78* (24), 8281–8289.
- (55) Middlebrook, A. M.; Bahreini, R.; Jimenez, J. L.; Canagaratna, M. R. Evaluation of Composition-Dependent Collection Efficiencies for the Aerodyne Aerosol Mass Spectrometer using Field Data. *Aerosol Sci. Technol.* **2012**, *46* (3), 258–271.
- (56) Canagaratna, M. R.; Jimenez, J. L.; Kroll, J. H.; Chen, Q.; Kessler, S. H.; Massoli, P.; Hildebrandt Ruiz, L.; Fortner, E.; Williams, L. R.; Wilson, K. R.; Surratt, J. D.; Donahue, N. M.; Jayne, J. T.; Worsnop, D. R. Elemental ratio measurements of organic compounds using aerosol mass spectrometry: characterization, improved calibration, and implications. *Atmos. Chem. Phys.* **2015**, *15* (1), 253–272.
- (57) Wang, C.; Wu, C.; Wang, S.; Qi, J.; Wang, B.; Wang, Z.; Hu, W.; Chen, W.; Ye, C.; Wang, W.; Sun, Y.; Wang, C.; Huang, S.; Song, W.; Wang, X.; Yang, S.; Zhang, S.; Xu, W.; Ma, N.; Zhang, Z.; Jiang, B.; Su, H.; Cheng, Y.; Wang, X.; Shao, M.; Yuan, B. Measurements of higher alkanes using NO+PTR-ToF-MS: significant contributions of higher alkanes to secondary organic aerosols in China. *Atmos. Chem. Phys.* **2020**, *20* (20), 1–32.
- (58) Wu, C.; Wang, C.; Wang, S.; Wang, W.; Yuan, B.; Qi, J.; Wang, B.; Wang, H.; Wang, C.; Song, W.; Wang, X.; Hu, W.; Lou, S.; Ye, C.; Peng, Y.; Wang, Z.; Huangfu, Y.; Xie, Y.; Zhu, M.; Zheng, J.; Wang, X.; Jiang, B.; Zhang, Z.; Shao, M. Measurement Report: important contributions of oxygenated compounds to emissions and chemistry of VOCs in urban air. *Atmos. Chem. Phys.* **2020**, *20* (20), 1–37.
- (59) Ye, C.; Yuan, B.; Lin, Y.; Wang, Z.; Hu, W.; Li, T.; Chen, W.; Wu, C.; Wang, C.; Huang, S.; Qi, J.; Wang, B.; Wang, C.; Song, W.; Wang, X.; Zheng, E.; Krechmer, J. E.; Ye, P.; Zhang, Z.; Wang, X.; Worsnop, D. R.; Shao, M. Chemical characterization of oxygenated organic compounds in gas-phase and particle-phase using iodide-CIMS with FIGAERO in urban air. *Atmos. Chem. Phys.* **2021**, *20* (20), 1–62.
- (60) Eluri, S.; Cappa, C. D.; Friedman, B.; Farmer, D. K.; Jathar, S. H. Modeling the formation and composition of secondary organic aerosol from diesel exhaust using parameterized and semi-explicit chemistry and thermodynamic models. *Atmos. Chem. Phys.* **2018**, *18* (19), 13813–13838.
- (61) Peng, Z.; Jimenez, J. L. Modeling of the chemistry in oxidation flow reactors with high initial NO. *Atmos. Chem. Phys.* **2017**, *17* (19), 11991–12010.
- (62) Atkinson, R.; Baulch, D. L.; Cox, R. A.; Crowley, J. N.; Hampson, R. F.; Hynes, R. G.; Jenkin, M. E.; Rossi, M. J.; Troe, J.; Subcommittee, I. Evaluated kinetic and photochemical data for atmospheric chemistry: Volume II – gas phase reactions of organic species. *Atmos. Chem. Phys.* **2006**, *6* (11), 3625–4055.
- (63) Zaytsev, A.; Koss, A. R.; Breitenlechner, M.; Krechmer, J. E.; Nihill, K. J.; Lim, C. Y.; Rowe, J. C.; Cox, J. L.; Moss, J.; Roscioli, J. R.; Canagaratna, M. R.; Worsnop, D. R.; Kroll, J. H.; Keutsch, F. N. Mechanistic study of the formation of ring-retaining and ring-opening products from the oxidation of aromatic compounds under urban atmospheric conditions. *Atmos. Chem. Phys.* **2019**, *19* (23), 15117–15129.
- (64) Wang, M.; Chen, D.; Xiao, M.; Ye, Q.; Stolzenburg, D.; Hofbauer, V.; Ye, P.; Vogel, A. L.; Mauldin, R. L.; Amorim, A.; Baccarini, A.; Baumgartner, B.; Brilke, S.; Dada, L.; Dias, A.; Duplissy, J.; Finkenzeller, H.; Garmash, O.; He, X.-C.; Hoyle, C. R.; Kim, C.; Kvashnin, A.; Lehtipalo, K.; Fischer, L.; Molteni, U.; Petäjä, T.;

- Pospisilova, V.; Quélér, L. L. J.; Rissanen, M.; Simon, M.; Tauber, C.; Tomé, A.; Wagner, A. C.; Weitz, L.; Volkamer, R.; Winkler, P. M.; Kirkby, J.; Worsnop, D. R.; Kulmala, M.; Baltensperger, U.; Dommen, J.; El-Haddad, I.; Donahue, N. M., Photo-oxidation of Aromatic Hydrocarbons Produces Low-Volatility Organic Compounds. *Environ. Sci. Technol.* **2020**, 54, 7911.
- (65) Xu, L.; Möller, K. H.; Crounse, J. D.; Kjaergaard, H. G.; Wennberg, P. O., New Insights into the Radical Chemistry and Product Distribution in the OH-Initiated Oxidation of Benzene. *Environ. Sci. Technol.* **2020**, 54, 13467.
- (66) Isaacman-VanWertz, G.; Massoli, P.; O'Brien, R.; Lim, C.; Franklin, J. P.; Moss, J. A.; Hunter, J. F.; Nowak, J. B.; Canagaratna, M. R.; Misztal, P. K.; Arata, C.; Roscioli, J. R.; Herndon, S. T.; Onasch, T. B.; Lambe, A. T.; Jayne, J. T.; Su, L.; Knopf, D. A.; Goldstein, A. H.; Worsnop, D. R.; Kroll, J. H. Chemical evolution of atmospheric organic carbon over multiple generations of oxidation. *Nat. Chem.* **2018**, 10 (4), 462–468.
- (67) Bruns, E. A.; Slowik, J. G.; El Haddad, I.; Kilic, D.; Klein, F.; Dommen, J.; Temime-Roussel, B.; Marchand, N.; Baltensperger, U.; Prévôt, A. S. H. Characterization of gas-phase organics using proton transfer reaction time-of-flight mass spectrometry: fresh and aged residential wood combustion emissions. *Atmos. Chem. Phys.* **2017**, 17 (1), 705–720.
- (68) Mehra, A.; Wang, Y.; Krechmer, J. E.; Lambe, A.; Majluf, F.; Morris, M. A.; Priestley, M.; Bannan, T. J.; Bryant, D. J.; Pereira, K. L.; Hamilton, J. F.; Rickard, A. R.; Newland, M. J.; Stark, H.; Croteau, P.; Jayne, J. T.; Worsnop, D. R.; Canagaratna, M. R.; Wang, L.; Coe, H. Evaluation of the chemical composition of gas-and particle-phase products of aromatic oxidation. *Atmos. Chem. Phys.* **2020**, 20 (16), 9783–9803.
- (69) Coggon, M. M.; Lim, C. Y.; Koss, A. R.; Sekimoto, K.; Yuan, B.; Gilman, J. B.; Hagan, D. H.; Selimovic, V.; Zarzana, K. J.; Brown, S. S.; Roberts, J. M.; Müller, M.; Yokelson, R.; Wisthaler, A.; Krechmer, J. E.; Jimenez, J. L.; Cappa, C.; Kroll, J. H.; de Gouw, J.; Warneke, C. OH chemistry of non-methane organic gases (NMOGs) emitted from laboratory and ambient biomass burning smoke: evaluating the influence of furans and oxygenated aromatics on ozone and secondary NMOG formation. *Atmos. Chem. Phys.* **2019**, 19 (23), 14875–14899.
- (70) Link, M. F.; Nguyen, T. B.; Bates, K.; Müller, J.-F.; Farmer, D. K. Can Isoprene Oxidation Explain High Concentrations of Atmospheric Formic and Acetic Acid over Forests? *ACS Earth and Space Chemistry* **2020**, 4 (5), 730–740.
- (71) Arey, J.; Obermeyer, G.; Aschmann, S. M.; Chattopadhyay, S.; Cusick, R. D.; Atkinson, R. Dicarbonyl Products of the OH Radical-Initiated Reaction of a Series of Aromatic Hydrocarbons. *Environ. Sci. Technol.* **2009**, 43 (3), 683–689.
- (72) Molina, M. J.; Ivanov, A. V.; Traktenberg, S.; Molina, L. T., Atmospheric evolution of organic aerosol. *Geophys. Res. Lett.* **2004**, 31 (22). DOI: 10.1029/2004GL020910
- (73) Malecha, K. T.; Nizkorodov, S. A. Photodegradation of Secondary Organic Aerosol Particles as a Source of Small, Oxygenated Volatile Organic Compounds. *Environ. Sci. Technol.* **2016**, 50 (18), 9990–9997.
- (74) Bianchi, F.; Kurtén, T.; Riva, M.; Mohr, C.; Rissanen, M. P.; Roldin, P.; Berndt, T.; Crounse, J. D.; Wennberg, P. O.; Mentel, T. F.; Wildt, J.; Junninen, H.; Jokinen, T.; Kulmala, M.; Worsnop, D. R.; Thornton, J. A.; Donahue, N.; Kjaergaard, H. G.; Ehn, M., Highly Oxygenated Organic Molecules (HOM) from Gas-Phase Autoxidation Involving Peroxy Radicals: A Key Contributor to Atmospheric Aerosol. *Chem. Rev.* **2019**, 119, 3472.
- (75) Roberts, J. M.; Veres, P. R.; Cochran, A. K.; Warneke, C.; Burling, I. R.; Yokelson, R. J.; Lerner, B.; Gilman, J. B.; Kuster, W. C.; Fall, R.; de Gouw, J. Isocyanic acid in the atmosphere and its possible link to smoke-related health effects. *Proc. Natl. Acad. Sci. U. S. A.* **2011**, 108 (22), 8966–8971.
- (76) Wang, Z.; Yuan, B.; Ye, C.; Roberts, J.; Wisthaler, A.; Lin, Y.; Li, T.; Wu, C.; Peng, Y.; Wang, C.; Wang, S.; Yang, S.; Wang, B.; Qi, J.; Wang, C.; Song, W.; Hu, W.; Wang, X.; Xu, W.; Ma, N.; Kuang, Y.; Tao, J.; Zhang, Z.; Su, H.; Cheng, Y.; Wang, X.; Shao, M. High Concentrations of Atmospheric Isocyanic Acid (HNCO) Produced from Secondary Sources in China. *Environ. Sci. Technol.* **2020**, 54 (19), 11818–11826.
- (77) Link, M. F.; Friedman, B.; Fulgham, R.; Brophy, P.; Galang, A.; Jathar, S. H.; Veres, P.; Roberts, J. M.; Farmer, D. K. Photochemical processing of diesel fuel emissions as a large secondary source of isocyanic acid (HNCO). *Geophys. Res. Lett.* **2016**, 43 (8), 4033–4041.
- (78) de Gouw, J.; Jimenez, J. L. Organic Aerosols in the Earth's Atmosphere. *Environ. Sci. Technol.* **2009**, 43 (20), 7614–7618.
- (79) Mao, J.; Ren, X.; Brune, W. H.; Olson, J. R.; Crawford, J. H.; Fried, A.; Huey, L. G.; Cohen, R. C.; Heikes, B.; Singh, H. B.; Blake, D. R.; Sachse, G. W.; Diskin, G. S.; Hall, S. R.; Shetter, R. E. Airborne measurement of OH reactivity during INTEX-B. *Atmos. Chem. Phys.* **2009**, 9 (1), 163–173.
- (80) Hayes, P. L.; Carlton, A. G.; Baker, K. R.; Ahmadov, R.; Washenfelder, R. A.; Alvarez, S.; Rappenglück, B.; Gilman, J. B.; Kuster, W. C.; de Gouw, J. A.; Zotter, P.; Prévôt, A. S. H.; Szidat, S.; Kleindienst, T. E.; Offenberg, J. H.; Ma, P. K.; Jimenez, J. L. Modeling the formation and aging of secondary organic aerosols in Los Angeles during CalNex 2010. *Atmos. Chem. Phys.* **2015**, 15 (10), 5773–5801.
- (81) Wang, C.; Yuan, B.; Wu, C.; Wang, S.; Qi, J.; Wang, B.; Wang, Z.; Hu, W.; Chen, W.; Ye, C.; Wang, W.; Sun, Y.; Wang, C.; Huang, S.; Song, W.; Wang, X.; Yang, S.; Zhang, S.; Xu, W.; Ma, N.; Zhang, Z.; Jiang, B.; Su, H.; Cheng, Y.; Wang, X.; Shao, M. Measurements of higher alkanes using NO<sub>x</sub> chemical ionization in PTR-ToF-MS: important contributions of higher alkanes to secondary organic aerosols in China. *Atmos. Chem. Phys.* **2020**, 20 (22), 14123–14138.
- (82) de Gouw, J. A.; Middlebrook, A. M.; Warneke, C.; Goldan, P. D.; Kuster, W. C.; Roberts, J. M.; Fehsenfeld, F. C.; Worsnop, D. R.; Canagaratna, M. R.; Pszenny, A. A. P.; Keene, W. C.; Marchewka, M.; Bertman, S. B.; Bates, T. S., Budget of organic carbon in a polluted atmosphere: Results from the New England Air Quality Study in 2002. *J. Geophys. Res.* **2005**, 110 (D16), DOI: 10.1029/2004JD005623.
- (83) Zhao, Y.; Nguyen, N.; Presto, A. A.; Hennigan, C. J.; May, A. A.; Robinson, A. L., Intermediate Volatility Organic Compound Emissions from On-road Gasoline Vehicles and Small Off-road Gasoline Engines. *Environ. Sci. Technol.* **2016**, 50, 4554.
- (84) Wu, L.; Wang, X.; Lu, S.; Shao, M.; Ling, Z. Emission inventory of semi-volatile and intermediate-volatility organic compounds and their effects on secondary organic aerosol over the Pearl River Delta region. *Atmos. Chem. Phys.* **2019**, 19 (12), 8141–8161.
- (85) Fang, H.; Huang, X.; Zhang, Y.; Pei, C.; Huang, Z.; Wang, Y.; Chen, Y.; Yan, J.; Zeng, J.; Xiao, S.; Luo, S.; Li, S.; Wang, J.; Zhu, M.; Fu, X.; Wu, Z.; Zhang, R.; Song, W.; Zhang, G.; Hu, W.; Tang, M.; Ding, X.; Bi, X.; Wang, X. Measurement report: Emissions of intermediate-volatility organic compounds from vehicles under real-world driving conditions in an urban tunnel. *Atmos. Chem. Phys.* **2021**, 21, 1–33.
- (86) Saha, P. K.; Khlystov, A.; Grieshop, A. P. Downwind evolution of the volatility and mixing state of near-road aerosols near a US interstate highway. *Atmos. Chem. Phys.* **2018**, 18 (3), 2139–2154.
- (87) Tsui, W. G.; Rao, Y.; Dai, H.-L.; McNeill, V. F. Modeling Photosensitized Secondary Organic Aerosol Formation in Laboratory and Ambient Aerosols. *Environ. Sci. Technol.* **2017**, 51 (13), 7496–7501.
- (88) Gkatzelis, G. I.; Coggon, M. M.; McDonald, B. C.; Peischl, J.; Aikin, K. C.; Gilman, J. B.; Trainer, M.; Warneke, C. Identifying Volatile Chemical Product Tracer Compounds in U.S. Cities. *Environ. Sci. Technol.* **2021**, 55 (1), 188–199.
- (89) Coggon, M. M.; Gkatzelis, G. I.; McDonald, B. C.; Gilman, J. B.; Schwantes, R. H.; Abu Hassan, N.; Aikin, K. C.; Arend, M. F.; Berkoff, T. A.; Brown, S. S.; Campos, T. L.; Dickerson, R. R.; Gronoff, G.; Hurley, J. F.; Isaacman-VanWertz, G.; Koss, A. R.; Li, M.; McKeen, S. A.; Moshary, F.; Peischl, J.; Pospisilova, V.; Ren, X.; Wilson, A.; Wu, Y.; Trainer, M.; Warneke, C. Volatile chemical product emissions enhance ozone and modulate urban chemistry. *Proc. Natl. Acad. Sci. U. S. A.* **2021**, 118 (32), No. e2026653118.

- (90) Lambe, A.; Massoli, P.; Zhang, X.; Canagaratna, M.; Nowak, J.; Daube, C.; Yan, C.; Nie, W.; Onasch, T.; Jayne, J.; Kolb, C.; Davidovits, P.; Worsnop, D.; Brune, W. Controlled nitric oxide production via O(1D) + N<sub>2</sub>O reactions for use in oxidation flow reactor studies. *Atmos. Meas. Tech.* **2017**, *10* (6), 2283–2298.
- (91) Lambe, A. T.; Krechmer, J. E.; Peng, Z.; Casar, J. R.; Carrasquillo, A. J.; Raff, J. D.; Jimenez, J. L.; Worsnop, D. R. HO<sub>x</sub> and NO<sub>x</sub> production in oxidation flow reactors via photolysis of isopropyl nitrite, isopropyl nitrite-d7, and 1,3-propyl dinitrite at  $\lambda=254$ , 350, and 369 nm. *Atmos. Meas. Tech.* **2019**, *12* (1), 299–311.
- (92) Peng, Z.; Palm, B. B.; Day, D. A.; Talukdar, R. K.; Hu, W.; Lambe, A. T.; Brune, W. H.; Jimenez, J. L., Model Evaluation of New Techniques for Maintaining High-NO Conditions in Oxidation Flow Reactors for the Study of OH-Initiated Atmospheric Chemistry. *ACS Earth and Space Chemistry* **2018**, 272

## □ Recommended by ACS

### Comprehensive Assessment for the Impacts of S/IVOC Emissions from Mobile Sources on SOA Formation in China

Junchao Zhao, Huan Liu, *et al.*

NOVEMBER 18, 2022

ENVIRONMENTAL SCIENCE & TECHNOLOGY

READ

### Mobile Sources Are Still an Important Source of Secondary Organic Aerosol and Fine Particulate Matter in the Los Angeles Region

Yunliang Zhao, Allen L. Robinson, *et al.*

OCTOBER 10, 2022

ENVIRONMENTAL SCIENCE & TECHNOLOGY

READ

### Upgrading Emission Standards Inadvertently Increased OH Reactivity from Light-Duty Diesel Truck Exhaust in China: Evidence from Direct LP-LIF Measurement

Qing'e Sha, Fei Yu, *et al.*

JUNE 30, 2022

ENVIRONMENTAL SCIENCE & TECHNOLOGY

READ

### Urban Oxidation Flow Reactor Measurements Reveal Significant Secondary Organic Aerosol Contributions from Volatile Emissions of Emerging Importance

Rishabh U. Shah, Albert A. Presto, *et al.*

DECEMBER 18, 2019

ENVIRONMENTAL SCIENCE & TECHNOLOGY

READ

[Get More Suggestions >](#)